

**MASARYKOVA UNIVERZITA**  
**PŘÍRODOVĚDECKÁ FAKULTA**  
ÚSTAV TEORETICKÉ FYZIKY A ASTROFYZIKY

# **Diplomová práce**

**BRNO 2012**

**ROBERT KLEMENT**



**MASARYKOVA UNIVERZITA**  
**PŘÍRODOVĚDECKÁ FAKULTA**  
ÚSTAV TEORETICKÉ FYZIKY A ASTROFYZIKY

---



# Určování vzdáleností dvojhvězd

Diplomová práce

**Robert Klement**

Vedoucí práce: doc. RNDr. Petr Hadrava, DrSc.

Brno 2012

# Bibliografický záznam

<b>Autor:</b>	bc. Robert Klement Přírodovědecká fakulta, Masarykova univerzita Ústav teoretické fyziky a astrofyziky
<b>Název práce:</b>	Určování vzdáleností dvojhvězd
<b>Studijní program:</b>	Fyzika
<b>Studijní obor:</b>	Teoretická fyzika a astrofyzika
<b>Vedoucí práce:</b>	doc. RNDr. Petr Hadrava, DrSc.
<b>Akademický rok:</b>	2011/2012
<b>Počet stran:</b>	vii + 40
<b>Klíčová slova:</b>	Zákrytové dvojhvězdy; Rozmotávání spekter; Vzdálenost k Malému Magellanovu Mračnu

# Bibliographic Entry

**Author:** bc. Robert Klement  
Faculty of Science, Masaryk University  
Department of Theoretical physics and astrophysics

**Title of Thesis:** Determination of Binary-Stars Distances

**Degree Programme:** Physics

**Field of Study:** Theoretical physics and astrophysics

**Supervisor:** doc. RNDr. Petr Hadrava, DrSc.

**Academic Year:** 2011/2012

**Number of Pages:** vii + 40

**Keywords:** Eclipsing binaries, disentangling of spectra, distance to the Small Magellanic Cloud

# Abstrakt

Předložená práce se zabývá způsobem určování vesmírných vzdáleností pomocí zákrytových dvojhvězd. Použita je metoda 'rozmotávání spekter', tj. výpočet orbitálních parametrů spolu s rozdělením pozorovaných spekter do spekter jednotlivých složek, pomocí softwaru vyvinutého vedoucím práce. Oproti předchozím studiím jsou zde použita i spektra pořízená během zákrytu a také části spektra kontaminované mezihvězdnou látkou. Účelem je rozpracování metodiky výpočtu hodnot orbitálních a astrofyzikálních parametrů včetně vzdálenosti a rozmotání čar mezihvězdné látky. Tato metodika byla užita pro čtyři vybrané dvojhvězdy a výsledky prokázaly její přednosti

# Abstract

In the present work we study the method of universal distance measurement using eclipsing binaries. We use the method of 'spectra disentangling', i.e. separation of the observed spectrum into components' spectra along with the calculation of orbital and stellar parameters, using software developed by the supervisor of this work. Unlike previous studies, spectra obtained during eclipses and parts of spectra contaminated by interstellar matter are used. The purpose is to develop a method of determining the values of orbital and astrophysical parameters including the distance and disentangling the lines of interstellar matter. The method was used for 4 selected binaries and the results proved its qualities.



**Masarykova univerzita**  
**Přírodovědecká fakulta**



## ZADÁNÍ DIPLOMOVÉ PRÁCE

**Student** : **Bc. Robert Klement, učo 269086**  
**Studijní program** : **Fyzika**  
**Studijní obor** : **Teoretická fyzika a astrofyzika**

Ředitel Ústavu teoretické fyziky a astrofyziky PŘF MU Vám ve smyslu Studijního a zkušebního řádu MU určuje diplomovou práci s tématem:


### Určování vzdáleností dvojhvězd

Determination of Binary-Stars' Distances

**Zásady pro vypracování:** Diplomant se bude zabývat metodologií určování vzdáleností dvojhvězd na základě jejich spektroskopie a fotometrie a jejím rozpracováním pomocí tzv. rozmotávání spekter.

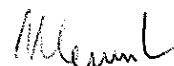
*Vedoucí diplomové práce* : RNDr. Petr Hadrava, CSc.  
*Datum zadání diplomové práce* : březen 2011  
*Datum odevzdání diplomové práce* : dle harmonogramu ak. roku 2011/2012

V Brně březen 2011

  
Michal L e n c  
ředitel ÚTFA

Zadání diplomové práce převzal dne:

Podpis studenta



# Poděkování

Na tomto místě bych chtěl poděkovat zejména vedoucímu své práce Petru Hadravovi za možnost spolupráce na zajímavém výzkumu. Dále děkuji Evropské Jižní Observatoři (ESO) za umožnění tříměsíční astronomické stáže v Santiagu, Chile. Z personálu ESO nejvíce děkuji Stanislavu Štefloví, který byl v ESO mým poradcem, a také Christophu Martayanovi za pomoc s redukcí dat. Děkuji také Přírodovědecké fakultě za finanční podporu při cestování do Chile a na konzultace do Prahy na Astronomický Ústav. Diplomová práce vznikla s podporou projektu specifického výzkumu číslo MUNI/A/0968/2009.

# Prohlášení

Prohlašuji, že jsem svoji diplomovou práci vypracoval samostatně s využitím informacích zdrojů, které jsou v práci citovány.

Brno 11. května 2012

.....  
Robert Klement

# Contents

<b>Chapter 1. Theoretical Introduction</b> .....	<b>1</b>
1.1 Eclipsing Binaries as Distance Indicators .....	1
1.2 The Ellipse Geometry and Orbital Parameters .....	4
1.3 Obtaining Stellar and Orbital Parameters from Spectra and Light Curves ..	7
1.4 Theory of spectra disentangling .....	9
1.5 The Codes Fotel, Korel and Bazant .....	12
1.6 Broader framework of the thesis project .....	13
<b>Chapter 2. Data used in the present study and their reduction</b> .....	<b>16</b>
2.1 Datasets used in the present study .....	16
2.2 Reduction of raw data from the FLAMES/GIRAFFE multi-object spectrograph .....	18
2.3 Possibilities to improve the previous studies .....	22
<b>Chapter 3. Disentangling of selected spectra</b> .....	<b>24</b>
3.1 Preparation of selected spectra for disentangling .....	24
3.2 The disentangling procedure .....	24
3.3 Results .....	26
3.3.1 SMC SC4-163552 .....	26
3.3.2 SMC SC5-38089 .....	26
3.3.3 SMC SC5-123390 .....	28
3.3.4 SMC SC6-17316 .....	28
<b>Chapter 4. Distance determination</b> .....	<b>35</b>
4.1 The method used for the calculation of distance .....	35
4.2 Conclusions .....	37
<b>Bibliography</b> .....	<b>38</b>



# Chapter 1

## Theoretical Introduction

### 1.1 Eclipsing Binaries as Distance Indicators

Deriving the distances of stellar objects is one of the most crucial steps in our understanding of the universe. The methods of measuring distances in the universe can be divided into two groups: Primary and secondary. Primary methods are based on a straightforward geometrical or physical principle, they do not need any calibration and can be used directly to measure the distance. Secondary methods are based on a more complicated astrophysical relation, which usually needs a primary distance marker to be properly calibrated. The primary methods of distance measurement are usually based on trigonometry or photometry.

Trigonometric methods are based only on the geometry of a given problem and there is no physics involved. The basic trigonometric method, which is also widely used for calibrating astrophysical relations needed to use other more far-reaching methods, is a trigonometric parallax. The basic idea is measuring the change of angular position of an object in the sky during the Earth's motion around the Sun. The mostly used trigonometric annual parallax  $\pi$  (we can also define e.g. a daily parallax) is defined as a difference in the object's angular position as seen from the Earth and from the Sun. Should this angular difference be measured, with the knowledge of the size  $d$  of the Earth's orbit and basic geometry, the distance  $D$  to the object can be easily calculated as

$$D = d/\pi . \tag{1.1}$$

In a similar way, the distance  $D$  to an object can be calculated if we know its linear size  $d$  and are able to measure its angular size  $\pi$ . The basic assumption for these methods is an Euclid space between the object and observer, which means we can neglect cosmological curvature or the influence of gravitational lensing.

However, because of the enormous distances in the universe, the parallax angles are so minute and difficult to measure, that the maximum distance possible to be determined in this way is very limited. Space missions HIPPARCOS and GAIA, designed to measure parallaxes of nearby stars in the Galaxy were launched outside the Earth's atmosphere, which helped greatly to increase the precision. Furthermore, ground-based interferometry can help a lot in increasing the possible reach of the parallax methods and in the near future, large interferometers should be able to measure distances to the Magellanic Clouds

[23]. Other types of parallaxes include dynamical parallaxes based on coherent motion of a group of objects, statistical parallaxes based on stellar motion in the Galaxy and pulsational parallax which measures pulsations of variable stars.

The methods based on photometry have proved to be more far-reaching in the so-called cosmic distance ladder than the trigonometric ones. If we want to be able to use the photometric methods we first have to know several laws about the propagation of light in space. The Euclid space is again an important assumption. The radiative flux  $F$  of an object is the total amount of light energy of all wavelengths that crosses a unit area perpendicular to the direction of light propagation per unit time. It depends on the object's intrinsic luminosity  $L$  (energy emitted per second) and the distance from observer. If we assume an object surrounded by a spherical shell of radius  $r$  and provided that no light is absorbed, we get the equation

$$F = \frac{L}{4\pi r^2}, \quad (1.2)$$

where the denominator is the area of the sphere. Therefore the radiative flux is inversely proportional to the square of the distance from the object, which is the inverse square law first suggested by Kepler. However, one has to include the effect of interstellar extinction, strongly dependent on the radiation wavelength, for real calculations. On its way between the emitting object and the observer, some photons can be absorbed or scattered by interstellar matter, which has a significant effect on the accuracy of the distance calculation. Therefore it is crucial to have a good estimate of the interstellar extinction.

The brightness of an object can be described by the logarithmic magnitude scale. The apparent magnitude  $m$  is the observed magnitude in a given distance and the absolute magnitude  $M$  is the apparent magnitude from the distance of 10 parsecs. The difference of 5 magnitudes between the apparent magnitudes of two objects corresponds to the smaller-magnitude star having 100 times higher flux than the larger-magnitude star. Therefore the flux ratio can be expressed as

$$\frac{F_2}{F_1} = 100^{(m_1 - m_2)/5}, \quad (1.3)$$

alternatively written as

$$m_1 - m_2 = -2.5 \log \frac{F_1}{F_2}, \quad (1.4)$$

which is called the Pogson equation. Combining the inverse square law (1.2) with equation (1.3), we get the connection between the object's apparent and absolute magnitude and its distance:

$$100^{(m-M)/5} = \frac{F_{10}}{F} = \left( \frac{d}{10\text{pc}} \right)^2, \quad (1.5)$$

where  $F_{10}$  is the flux received in the distance of 10 parsecs and  $d$  is the distance in parsecs. When we solve for  $d$  and use logarithm on both sides of the equation, we get a relation for the object's distance modulus  $m - M$ :

$$m - M = 5 \log d - 5 = 5 \log \frac{d}{10\text{pc}} \quad (1.6)$$

It is clear that for the calculation of the distance  $d$  the absolute magnitude  $M$  is needed. Standard candles are objects with known absolute magnitudes and should we be able to

identify the type of a standard candle (usually they have a specific light curve), the distance can be calculated using the inverse square law. However, the distance to at least one near standard candle has to be estimated by a different method to be able to calculate its absolute magnitude. This task can be quite difficult, as will be seen from the following examples.

The most known primary method based on photometry is the famous period-luminosity (P-L) relation of Cepheids. Cepheids are very bright pulsating variable stars, which means they change their magnitude together with their dimensions. At the beginning of the twentieth century, some Cepheids were discovered and observed in the Small Magellanic Cloud and a linear dependence of the mean apparent magnitude on the period in logarithmic scale was found out (Cepheids observed in SMC were assumed to be roughly in the same distance). That means that by measuring the pulsational period of a Cepheid in an unknown distance, we can calculate the apparent magnitude that the star would have if it was in the same distance as the comparison Cepheid and by comparing the calculated apparent magnitude to the observed one, we get the ratio of distances of the comparison and observed Cepheid. Therefore, the relation can be used to measure the relative distances of different Cepheids, but to get the actual distance from the observer, the distance to a near Cepheid has to be first found out by a different and precise method. This proved to be a difficult task, as even the nearest Cepheid, Polaris, is so far away that its trigonometric parallax was hard to measure precisely (until the launch of Hipparcos). Another problem with the Cepheid method is that the P-L relation depends on metallicity, which means that when the Cepheids are observed in other galaxies, their period-luminosity relation can be different from the one found out originally. The calibration can be again made by measuring the distance of at least two Cepheids using other primary methods (which in this case essentially makes the Cepheid method not a primary one) but fortunately there are methods, such as the Baade-Wesselink method, allowing us to obtain the P-L relation directly. Other photometric methods using variable stars include the absolute magnitude - metallicity relation of RR Lyrae variables and P-L relation of Mira variables [6].

Type Ia supernovae are also standard candles. The same value of their absolute magnitude comes from the fact that they light up at a specific moment, when a white dwarf star reaches the Chandrasekhar mass limit. Above the limit, the degenerated electron pressure is not able to resist the gravitational pressure and nuclear reactions energetic enough to blow the star apart are lit. This usually happens in a close binary system, where matter from one component accretes to the other one. Ia supernovae have a specific light curve and they can be identified in very distant galaxies, allowing us to calculate their distance. X-ray bursts from the surface of neutron stars and novae are other examples of standard candles.

The importance of eclipsing binaries among previous methods of distance determination is unquestionable. Eclipsing binaries are binary stars which have orbital planes oriented approximately along the observer's line of sight. As they are orbiting their center of mass, they periodically eclipse each other, causing variations in the amount of light observed. It is originally a photometric method, but interferometry has recently made it possible for the distance of a bright binary to be determined purely geometrically by measuring separation of the two stars in the sky. The star Atlas, located in Pleiades, is such a visual and spectroscopic binary. There has been a controversy concerning the distance to this star and to the Pleiades cluster, as the results differed when using the method of main

sequence fitting and using the trigonometric parallax obtained by Hipparcos [24]. The purely geometrical measurement helped to resolve this controversy in favour of the main sequence fitting, discovering a serious problem with the Hipparcos parallax measurements [33].

This work, however, will be dealing with the traditional method of distance determination, which is based on photometric and spectroscopic observations, and is discussed in detail in the following subchapter. For this method, the eclipsing binary must also be a spectroscopic one. Orbital motion of a spectroscopic binary has a component along the line of sight, which results in periodic shifts of spectral lines in the blended spectra. The components should have similar luminosities for lines of both components to be visible (these binaries are called double-line, eclipsing, and spectroscopic ones). Then it is possible to measure the radial velocities, which are essential for the method. In the cosmic distance ladder, eclipsing binaries play a fundamental role, as they are very common and a vast number of them have recently been discovered in nearby galaxies. Eclipsing binaries can be used not only to measure the Galactic distances, but also, as proved by more recent studies (e.g. [3]), to measure distances to the closest large spiral galaxies M31 and M33, which enables a precise calibration of secondary methods based on properties of galaxies.

Main sequence fitting is a method based on determining the spectral types of a group of stars. If these stars are in their hydrogen-burning period, they are on the main sequence in the Hertzsprung-Russel diagram. The H-R diagram is an absolute magnitude to spectral type dependence, absolute magnitudes of the observed stars can be determined and therefore also their distance.

There are also methods, which are less precise but which can be used to measure enormous distances, such as the Globular Cluster Luminosity function, which is used to compare the luminosities of globular clusters orbiting galaxies in known distance to the luminosities of globular clusters orbiting galaxies further away.

## 1.2 The Ellipse Geometry and Orbital Parameters

To understand the way of deriving orbital parameters of binary stars from spectra and light curves, it is first crucial to understand the geometry of ellipse and the way in which the components of binary stars orbit each other. When Kepler was analyzing Brahe's observations in order to support the heliocentric model of the Solar system, he was not only forced to admit that it is the planets that orbit the Sun, but he also had to accept that the orbits were not perfectly circular. His analysis led him in 1609 to publishing his first two laws, the first one stating that planets orbit the Sun in an ellipse, with the Sun at one of its foci and the second one stating that a line connecting a planet to the Sun sweeps out equal areas in equal time intervals. We now know that ellipse is in fact a special case of orbit and that two celestial objects can follow an orbit of any conic section, namely a circle and an ellipse for a closed orbit and a parabola or a hyperbola for an open orbit. When observing binary stars, the orbits are generally elliptical, but often the orbits are nearly circular as (mostly close) binaries tend to circularize their orbits through tidal interaction.

The ellipse is a planar curve defined as a set of points with a constant sum of distances from two points called foci. The most important characteristic of an ellipse is its eccentricity  $e$ . On Fig. 1.1 the distance from the center  $C$  to the foci  $F1$  or  $F2$  is equal to the product  $ae$ ,

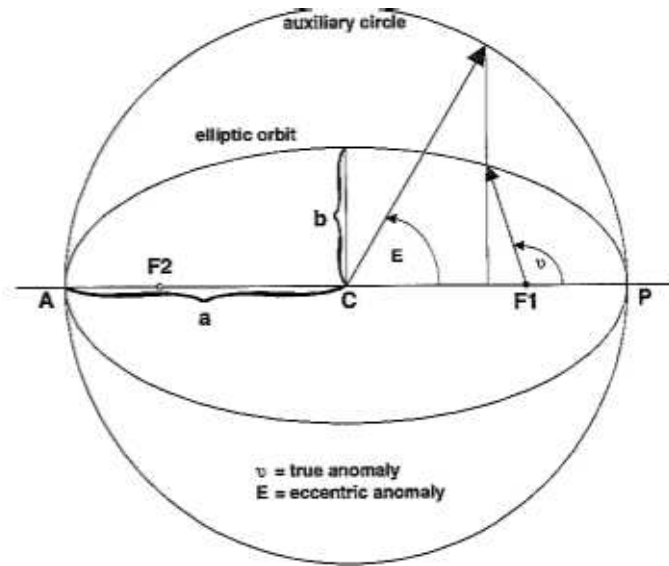


Figure 1.1: Ellipse geometry

where  $a$  is the semimajor axis. Therefore the eccentricity is a number between 0 (ellipse becoming a circle) and 1 (ellipse becoming a line). The point P is called periastron and it corresponds to the closest approach of orbiting objects. Another important aspect of an ellipse is the true anomaly  $v$ , which is related to the eccentric anomaly  $E$  as

$$v = \arctan \left( \sqrt{\frac{1+e}{1-e}} \tan \frac{E}{2} \right), \quad (1.7)$$

and  $E$  is related to the mean anomaly  $M$  via Kepler's equation

$$E - e \sin E = M \quad (1.8)$$

The mean anomaly is a mathematically convenient quantity that changes linearly with time and it relates the position of a body on the orbit with a specific epoch. It does not correspond to any real geometric angle, but can be converted into eccentric or true anomaly in the way outlined above.

When we consider orbits of binary stars, we have to distinguish between absolute and relative orbits. When we talk about absolute orbits, we assume that the two components of a binary orbit around a common center of mass, with two ellipses with semimajor axes  $a_1$  and  $a_2$  describing the orbital motion. Therefore it is useful to define a relative orbit, which describes the orbital motion of one component relative to its (more massive) companion's center of mass. This orbit is then described by only one ellipse with a semimajor axis  $a = a_1 + a_2$ . The Keplerian orbital motion can be expressed as

$$r = \frac{a(1-e^2)}{1+e \cos v}, \quad (1.9)$$

where  $r$  is the distance of one component from the other one's center of mass.

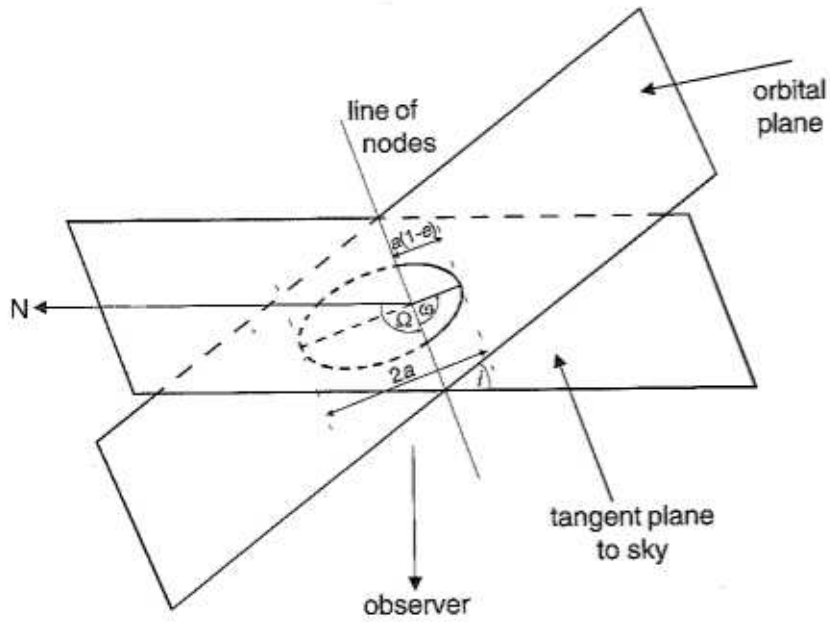


Figure 1.2: Orbital elements

Ten years after publication of his first two laws, Kepler published the so-called Harmonic law, which states that the second power of orbital period  $P$  is proportional to the third power of orbit's semimajor axis  $a$ . In a precise form, this is expressed by equation

$$P^2 = \frac{4\pi^2}{G(M_1 + M_2)} a^3, \quad (1.10)$$

where  $M_{1,2}$  are masses of the component stars and  $G$  is the gravity constant.

The third Kepler's law is one of the most important laws in astronomy as it provides the most direct way of calculating masses of celestial objects. Among other applications, it is used to calculate the masses of components of binary stars if we know their orbital period and the absolute size of the orbit.

If we want to fully describe a relative orbit of a binary star, we need to know the Keplerian orbital elements (Fig. 1.2). The first two are related to the shape of orbital ellipse: the semimajor axis  $a$  and the eccentricity  $e$ . Next is the orbital inclination  $i$  equal to  $90^\circ$  when we see the orbit from side and to  $0^\circ$  when we see it from the top and the longitude of the ascending node  $\Omega$  determining the angular position of the intersection of the orbital ellipse with the reference plane (a tangent plane to the sky). Then there is the argument of periastron  $\omega$  which is the angular distance of periastron from the ascending node in the direction of motion, the epoch of periastron passage  $T_0$  and the orbital period  $P$ .

### 1.3 Obtaining Stellar and Orbital Parameters from Spectra and Light Curves

The method of measuring the distance of a double-line, eclipsing, spectroscopic binary dates back about a century (the history of the development and use of the method can be found in [19]). Both the light curves originating from photometry and the radial velocity curves from spectroscopy are needed. The method is mostly photometric, with only one relation needed to be estimated from the theory of stellar atmospheres. It is the relation between the temperatures and surface luminosities of the binary components. Other stellar parameters can be obtained directly from the light curves and spectra.

Let us first focus on analyzing the light curve. The light curve is a graph showing the object's (usually a variable star) magnitude dependence on time. In the simplest case of an eclipsing binary without any proximity effects it is a straight line showing two minima corresponding to the two eclipses. If the components of a binary with circular orbit have different temperatures (and consequently the specific intensity of surface radiation), the depths of the minima are also different, therefore we observe the so-called primary and secondary minima. The deeper primary minimum corresponds to the cooler component eclipsing the hotter one (for main sequence stars, the hotter star also has a larger radius, therefore this eclipse is a partial one) and the secondary minimum corresponds to the hotter component eclipsing the cooler one. For eccentric orbits, the differences in projected distances of star centers may also influence the depths of the eclipses. The light curve of an eclipsing binary is usually drawn only during one period and the time dependence is exchanged for the orbital phase dependence (with the phase equal to one corresponding to one full orbit). From the analysis of a light curve of a given binary, we can get well-constrained information about the orbital period and inclination of the orbit. The period can be calculated directly from the time difference between two consecutive primary or secondary eclipses. The longer the time of photometrical observation, the more minima occur and the period can be calculated more precisely. The inclination of the orbit can be obtained from analysing the shapes of minima. For inclination being close to the ideal value of  $90^\circ$ , at least one of the eclipses is a total one, therefore the minimum corresponding to it will be constant. For inclination differing from  $90^\circ$ , the eclipses are usually partial only and the minima are sharp and no longer constant. The durations of the primary and secondary minima indicate the components' radii scaled to the size of the orbit and also the ratio of surface luminosities can be estimated [23, 15].

The radial velocity curves (RV curves), which are usually calculated from the shifts of specific lines of the components' spectra (several methods are outlined in the following subchapter), yield information about the velocity semi-amplitudes  $K_{1,2}$ . From the semi-amplitudes we immediately know also the mass ratio, as  $\frac{K_1}{K_2} = \frac{M_2}{M_1} = q$ . From the shape of RV curves it is also possible to determine eccentricity  $e$  (to a certain extent eccentricity can be derived from the light curve as well, but the RV curves constrain the information better). For a circular orbit, the radial velocity curves are sinusoidal. The orbital inclination does not change the shape of the curves, but only their amplitudes by a factor  $\sin i$ . When the orbit is eccentric, radial velocity curves are no longer sinusoidal and become skewed. From the exact shape of the curves, eccentricity and periastron longitude can be calculated. But fortunately, many close binaries tend to circularize their orbits, therefore making the

analysis easier. If we assume almost circular orbits ( $e \ll 1$ ), the orbital velocities are constant and connected to the component masses:

$$\frac{M_1}{M_2} = \frac{v_2}{v_1} \quad (1.11)$$

Because the radial velocities can be calculated as  $v_r = v \sin i$ , the mass ratio can be calculated without the knowledge of orbital inclination:

$$\frac{M_1}{M_2} = \frac{v_{2r}/\sin i}{v_{1r}/\sin i} = \frac{v_{2r}}{v_{1r}} \quad (1.12)$$

When we combine the radial velocities with the period and inclination obtained from the light curve, the absolute size of the orbit can be calculated (the semimajor axis  $a$ )

$$a = a_1 + a_2 = \frac{P}{2\pi}(v_1 + v_2), \quad (1.13)$$

as well as linear radii  $R_{1,2}$  of the components. Then, using the third Kepler's law (1.10) and with the mass ratio  $q$  known, also the masses can be found out. For circular orbits the law (1.10) becomes:

$$M_1 + M_2 = \frac{P}{2\pi G} \frac{(v_{1r} + v_{2r})^3}{\sin^3 i} \quad (1.14)$$

Therefore, for the absolute masses to be calculated, the orbital inclination is needed.

Then the most complicated step of the method comes: The surface brightnesses have to be estimated. For that, we need to know the effective temperature, which can be calculated when photometry in different bands is available (this can also be used to calculate the interstellar reddening), or using the separated component spectra (from the continuum ratios or from line-strength ratios). If we consider the star to be a black body, it emits electromagnetic radiation according to Planck's law, which can be expressed in terms of the radiation frequency as:

$$B_\nu(T) = \frac{2h\nu^3}{c^2} \frac{1}{\exp(\frac{h\nu}{k_B T}) - 1}, \quad (1.15)$$

where  $B_\nu$  is the energy radiated at frequency  $\nu$  from unit area,  $h$  is the Planck constant,  $c$  is the speed of light,  $k_B$  is the Boltzmann constant and  $T$  is the surface temperature. If we integrate this expression over all frequencies and over the solid angles corresponding to a hemisphere above the surface, we get the Stefan-Boltzmann law:

$$L = \sigma T_{eff}^4, \quad (1.16)$$

where  $\sigma = \frac{2k_B^4\pi^5}{15c^2h^3}$  is the Stefan-Boltzmann constant. The Stefan-Boltzmann law states the total luminosity  $L$ , i.e. the total energy radiated from unit area of an object with effective temperature  $T_{eff}$ . Therefore the expression:

$$L = 4\pi R^2 \sigma T_{eff}^4, \quad (1.17)$$



states the total luminosity of an object of radius  $R$  and effective temperature  $T_{eff}$ . Then, finally, the distance can be calculated from the inverse square law [23].

The ideal eclipsing binary, thought traditionally to be the best distance indicator, is composed of two stars of similar temperature and luminosity, with their distance significantly larger than radii. Also, the orbit should not be too eccentric [7]. These binaries can be assumed to be spherical and there is no need to be concerned about mass transfer between the components and other effects resulting from the components being too close to each other. However, according to [32], detached binaries with proximity effects, semi-detached binaries and even contact ones, constrain the stellar parameters and therefore the distance even better.

## 1.4 Theory of spectra disentangling

In the past, spectra of binary stars were obtained using photographic plates as detectors. Radial velocities of the components were then calculated by measuring the difference between positions of stellar lines and comparison lines using instruments like the Abbe comparator. Since then the methods of RV measurement have improved a lot and some of them allow for the full spectra disentangling, i.e. separation of the observed spectrum into component spectra along with the calculation of orbital and stellar parameters.

One of the methods of measuring the radial velocities on which disentangling is based is the method of cross-correlation [17]. The idea of cross-correlation is to compare the observed spectrum with a template spectrum, which should essentially be the same as the observed one apart from the Doppler shifts caused by radial motion. The template spectrum can be a spectrum of a comparison star of the same spectral type or a synthetic spectrum created by modelling the stars' atmospheres. In the form of an equation, the cross-correlation can be expressed as

$$F(v) \equiv \int I(x+v)J(x)dx, \quad (1.18)$$

where  $I(x)$  is the observed spectrum and  $J(x)$  the chosen template. Maxima of the resulting function  $F(v)$  then indicate the radial velocity shifts  $v$  corresponding to the template spectral features detected in the observed spectrum. It is important to use the logarithmic wavelength scale

$$x = c \ln \lambda, \quad (1.19)$$

in which the Doppler shifts are equivalent for all wavelengths (this holds also for the following method as well as for the disentangling). The need for a template spectrum essentially makes this method a problematic one as it is sometimes not easy to estimate it. A way to avoid this problem is to use blended spectrum of the same binary taken near conjunction as a template, if the components are of a similar spectral type. A similar method using a template spectrum is the method of broadening function [26] expressed as

$$I = B * J, \quad (1.20)$$

where  $B$  is the broadening function to be solved by deconvolution. Should the template match the intrinsic stellar spectrum exactly, it is a Dirac delta function shifted for the radial

velocity. Generally, it can also include broadening of the line-profiles of the observed spectrum due to e.g. rotation effect. However, the problem with the need of using a template spectrum remains.

The first true disentangling method was introduced by Simon & Sturm [30]. The method is based on solving the set of linear equations, represented by a product of a linear transformation matrix  $M$  and the component spectra  $I_A, I_B$  being equal to the composite spectra  $I(t)$ :

$$\begin{pmatrix} M_{A1} & M_{B1} \\ \vdots & \vdots \\ M_{AN} & M_{BN} \end{pmatrix} \begin{pmatrix} I_A \\ I_B \end{pmatrix} = \begin{pmatrix} I(t_1) \\ \vdots \\ I(t_N) \end{pmatrix} \quad (1.21)$$

For a binary star this system of equations is overdetermined if we use three or more composite spectra observed at different phases. The exposures should not be taken during eclipses, as it is assumed that spectra and the light ratio do not vary with phase. The continuum levels of component spectra can not be derived, hence a photometric observation is needed. For the matrix  $M$  to have a simple form of a set of unit submatrices with diagonals shifted for the corresponding value of radial velocity, rebinning the input data into an equidistant wavelength scale is needed. The system of linear equations is solved using the numerical method of singular value decomposition. The main improvement over previous methods is no need for template spectra, as all the exposures are mutually compared during the calculation.

The disentangling method developed by P. Hadrava [9] has a similar principle, the main difference being the use of Fourier image of the input spectra. This method solves for the radial velocities which are functions of parameters characterizing orbital motions of the components (orbital elements) or physical and geometrical conditions of formation of their spectra. Therefore it is possible to directly fit these parameters from the observed spectra. A by-product of the calculation are the mean component spectra for each exposure. A necessary assumption is that the radial velocities are given by a known law of orbital motion. The calculation itself is based on least-squares fitting of transformed spectra with direct analytical calculation of linear coefficients and optimization in the non-linear ones.

In the simplest case with the component spectra being constant in time, the observed spectrum  $I(x, t)$  can be expressed by the convolution:

$$I(x, t) = \sum_{j=1}^n I_j(x) * \delta(x - v_j(t)), \quad (1.22)$$

where  $I_j(x)|_{j=1}^n$  are the component spectra of  $n$  stars Doppler shifted for instantaneous radial velocity  $v_j(t)$  of the star  $j$  at the time  $t$  and the variable  $x$  is logarithmic in wavelength (equidistant in radial velocities),  $x = c \ln(\lambda)$ . The Fourier transform of this equation is:

$$\tilde{I}(y, t) = \sum_{j=1}^n \tilde{I}_j(y) \exp(iy v_j(t)). \quad (1.23)$$

If we have  $k$  spectra ( $k > n$ ) observed at times  $t_l|_{l=1}^k$  corresponding to radial velocities  $v_j(t_l)$ , it is possible to fit them searching for appropriate values of  $v_j(t_l)$  and  $\tilde{I}_j(y)$ , where  $v_j(t_l)$  are functions of parameters  $p$ . The least squares fits in  $x$  and  $y$  spaces are equivalent,

following from the Parseval theorem ( $\int |\tilde{f}(y)|^2 dy = 2\pi \int |f(x)|^2 dx$ ). Therefore the sum of squares  $S$  to be minimized can be written as:

$$S = \sum_{l=1}^k \int \left| \tilde{I}(y, t_l) - \sum_{j=1}^n \tilde{I}_j(y) \exp(iy v_j(t_l; p)) \right|^2 dy. \quad (1.24)$$

By varying the sum  $S$  with respect to individual Fourier modes, we obtain a set of  $n$  linear equations for each Fourier mode. This fact makes the disentangling of observed spectra easier in comparison to disentangling in the wavelength domain. By solving these sets of equations we obtain the radial velocities  $v_j(t_l)$  and parameters  $p$ .

In practise, only limited spectral regions containing needed spectral features are selected for the disentangling in order to achieve a good resolution in radial velocity. It is important to have the edges of these regions close to continuum because if there was a line at the edge, the periodicity of Fourier transform would expect it to appear on the other edge when Doppler shifted out of the region.

Several generalizations which include calculating with line-strength variations, limb darkening, intrinsic line-profile variations and broadening by pulsations, have been introduced to the Fourier mode disentangling technique ([10][11][12]). With the line-strength variation included, delta functions  $\delta(x - v_j(t))$  representing the Doppler shifts are replaced by a product  $s_j(t)\delta(x - v_j(t))$  where the factors  $s_j(t)$  can be fitted to the data to find the variations in strengths of lines. This is important when using exposures obtained close to conjunctions, as during eclipses the component spectra are combined in a different proportion. Without a line-strength variation included, radial velocities calculated using these exposures suffer from a much larger scatter. An important fact is that the line-strengths of an eclipsed component do not necessarily need to decrease as one would expect, but may be enhanced due to limb-darkening during a partial eclipse. This can be explained by the fact that when the limb area of a stellar disk is eclipsed and only the inner part can be seen, there is more light missing from the absorption lines originating in the photosphere than from the continuum, making the absorption lines even deeper. This fact makes the interpretation of the  $s_j(t)$  factors somewhat complicated. Apart from the possible use of eclipsed spectra without any loss in precision, this generalization also in principle enables disentangling of telluric and interstellar lines.

In a more general case where line profiles could be variable, delta functions in the products  $s_j(t)\delta(x - v_j(t))$  representing the Doppler shifts are exchanged for some general broadening functions  $\Delta_j(x, t, p)$ . The variation of  $S$  could be done with respect to the parameters  $p$  themselves, but as the dependence of  $\tilde{\Delta}_j(y, t, p)$  on  $p$  can be complicated, it is more convenient to minimize  $S$  with respect to  $\tilde{I}_j(y)$  and use a numerical method of optimization to solve for  $p$ . An important note is that the continua of observed spectra cannot be directly decomposed as they are not influenced by the Doppler shifts.

The generalizations introducing disentangling with intrinsic line-profile variations due to e.g. cepheid pulsations and rotational effect (e.g. [14]) represent another important progress in the interpretation of spectra of spectroscopic binaries. However, these were not used in the present study.

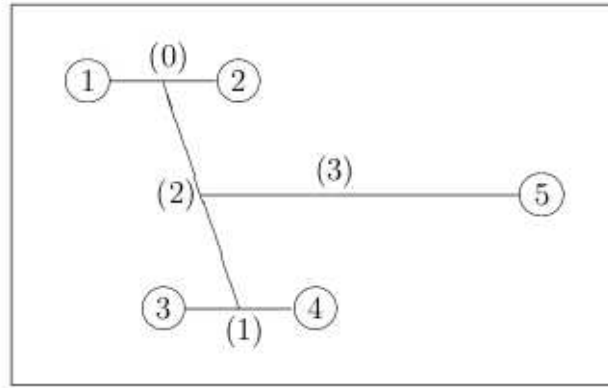


Figure 1.3: The hierarchical structure of a stellar system used in Korel. Numbers in brackets denote numbers of orbits and numbers in circles denote the numbers of components. All components do not have to be stellar, but can represent also a circumstellar or interstellar matter.

## 1.5 The Codes Fotel, Korel and Bazant

Fotel is a fortran code written by P.Hadrava (prior to developing the Fourier disentangling method) for solution of photometric elements of eclipsing binaries. Both the radial velocity curves and the light curves in different colour bands can be used as an input, together with additional datasets such as the angular distance between the binary components, the position angle and the timing of minima. Fotel assumes the geometry and the orbital motion as outlined in Section 1.2. The solution of orbital elements and other parameters is based on the minimization of the sum of  $(O - C)$  as a function of the elements. As some orbital parameters are more sensitive to either the RV curves or the light curves (RV curves do not give information about the inclination and the light curves are typically insensitive to the mass ratio and less sensitive to the eccentricity), the minimization of the sum  $(O - C)$  can be done simultaneously for all datasets and their influence can be adjusted by appropriate choice of the dataset weights. The minimization in non-linear parameters is done by the numerical simplex method [18]. Up to 20 parameters can be chosen to converge at once. For the calculation it is possible to choose between radiation in the approximation of three-axial ellipsoid shapes of the component stars or the more complex shapes of stars in the Roche model. Apart from the calculation of the basic Keplerian orbital elements, i.e. the period  $P$ , periastron epoch  $T_0$ , eccentricity  $e$ , periastron longitude  $\omega$ , amplitude of RV  $K_1$ , mass ratio  $q$  and from the light curve only the inclination  $i$ , the components' radii in units of the semimajor axis  $R_1$  and  $R_2$  and the colour magnitude of one of the components  $m_\lambda$ , the model embedded in Fotel includes more subtle parameters such as the third light (or a possible third component, including its orbital elements and radius), components' limb darkening coefficients, albedos, gravity darkening coefficients and others. For detailed overview, see the FOTEL4 User's guide [13].

Korel is a fortran code enabling the use of the method of Fourier domain spectra disentangling of spectroscopically variable stellar systems outlined in the previous section. The hierarchical structure of the stellar system used in Korel can be seen in Fig. 1.3. For

detailed theory and also a manual for Korel, see Disentangling of spectra - theory and practise [12].

Bazant, the merging of Fotel and Korel into one code has been under development for some time and although it has not been published at the time of writing this thesis, a preliminary version was provided to me by its author. One of the purposes of the present work was to test the run of this code and to help debugging it. All the results presented here were calculated using Bazant, which allows for simultaneous solution for the light curves, radial velocities and observed spectra. What has been outlined above for Fotel and Korel stands also for Bazant, with the observed spectra being treated as a separate dataset with adjustable weight.

## 1.6 Broader framework of the thesis project

Small Magellanic Cloud (SMC) and Large Magellanic Cloud (LMC) are dwarf irregular galaxies forming an interacting system with the Milky Way (MW). Apart from their smaller size and different shape, the main differences from the MW are their high content of gas and a lower heavy element abundance resulting in a lower dust content and a stronger interstellar radiation field [29]. The formation and evolution of the Magellanic system has been a subject of scientific interest for a long time and there have been some controversies associated with its origin, three-dimensional structure and depth along the line of sight. It has been a target of several radio surveys of HI 21cm emission (most recently [4]), revealing a large filamentary gaseous structures, possible remnants of the past LMC-SMC-MW interaction, extending to both high negative and positive Local State of Rest radial velocities (Fig. 1.5). These structures include a common envelope in which SMC and LMC are embedded, the Magellanic Bridge connecting them, the Magellanic Stream - a huge gaseous tail spreading across  $\approx 100^\circ$  of the plane of sky- , the Leading Arm and the Interface Region (Fig. 1.4). The history of interaction of the Magellanic System with the MW has been a subject of complex dynamical modeling with a sophisticated model using the Genetic Algorithm for searching for the free parameters being introduced recently by Ruzicka et al. ([27, 28]). This model includes such parameters as a shape and extension of the dark matter halo around the MW.

The results presented in this work are a part of precise measurements of spacial and kinematic structure of Magellanic Clouds, which will be used to further develop the mentioned dynamical model, specifically to put more constraints on some free parameters. In order to do that it is important to obtain not only the depth structure of the stellar components of the SMC but also of the interstellar matter. Unfortunately, the radio surveys provide distribution in the right ascension, declination and radial velocity only, providing no information on the real three-dimensional structure. However, our method of spectra disentangling allows not only to separate the spectra of the binary components, but also (if present) the emission of the circumstellar HII and the absorption of the interstellar HI matter including, naturally, emission or absorption in lines not only of hydrogen but also of ions of heavier elements. This would not be possible for single stars without changes in their radial velocity. By disentangling the interstellar absorption, it is possible to put an upper limit on the distance of the HI interstellar gas (in which the absorption originates) in corresponding part of its RV-distribution. This is a novelty of this project

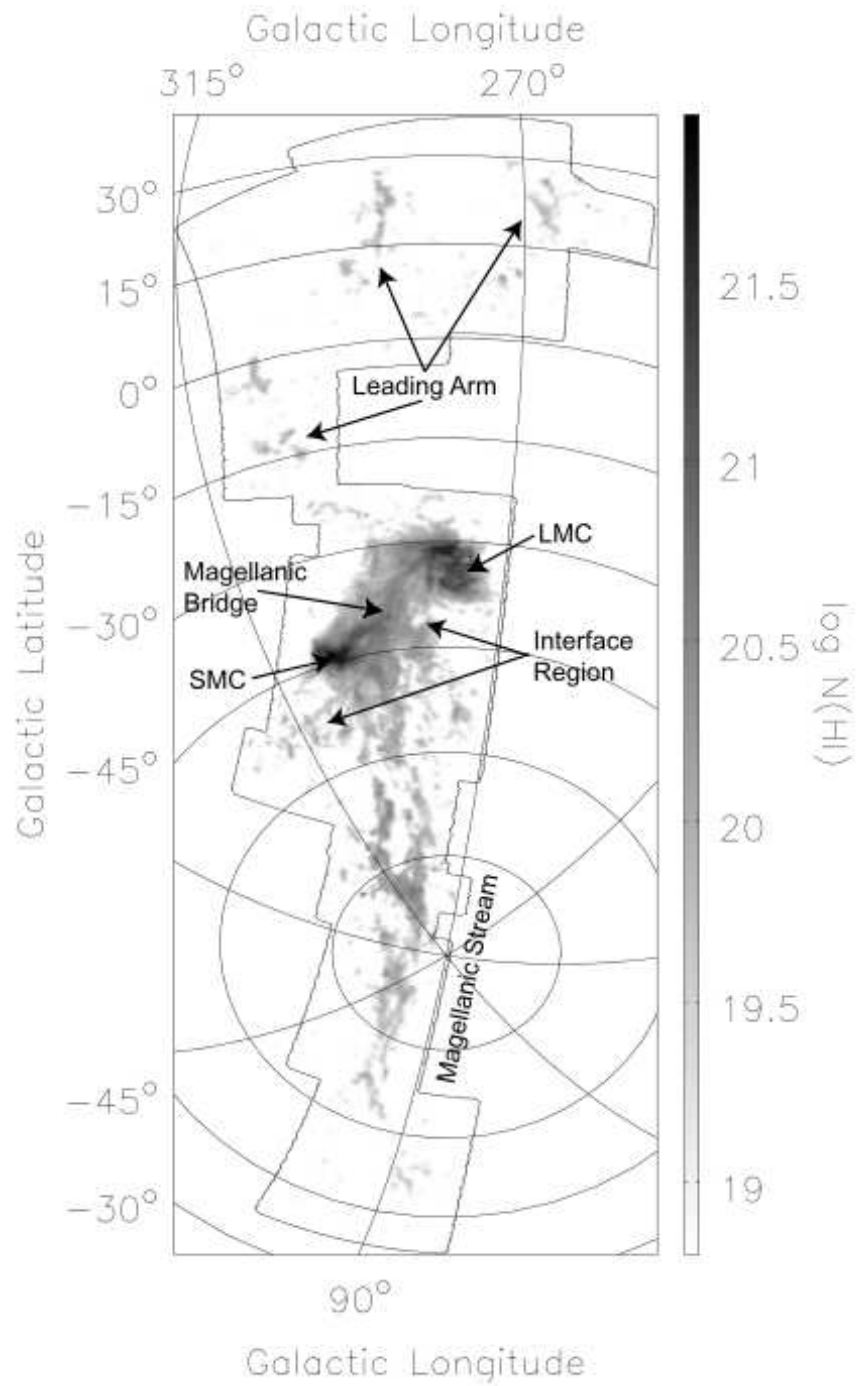


Figure 1.4: HI column density distribution in the Magellanic System [4]

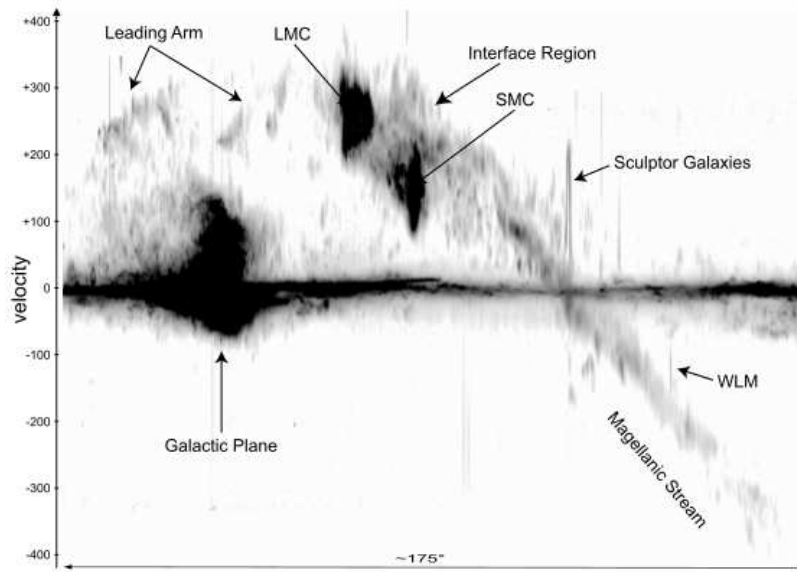


Figure 1.5: Position/velocity peak intensity map of the Magellanic System. The position corresponds to the y-axis in Fig. 1.4 [4]

unattainable by any other known method which should help answering open questions about the SMC-LMC-MW interaction history. The strength of interstellar absorption lines also enables to determine the column density of ISM, the consequent extinction and thus to improve the distance of the star. The upper limit of distance is not available for the ISM emission lines as the emission may originate further than the stellar spectrum, but their disentangling is needed to measure correctly the stellar parameters and radial velocities of emission lines may also yield interesting information about the kinematics of the HII gas in the SMC. By-products will be an observational test of mass-radius-luminosity relations for massive low-metallicity stars predicted by theoretical evolutionary models, and test of the methods of primary distance measurements.

In the large picture, the main goal is to yield important constraints on galactic physics and cosmology - tidal evolution, the total mass including dark matter, star-formation etc. The mapping of depth and radial velocity structure of SMC will be used to explore the history of interaction between the Magellanic Clouds and the Milky Way, and possibly answer the question whether it is the first encounter of SMC with the MW on a hyperbolic orbit, or if SMC periphery is mainly perturbed by the LMC.

## Chapter 2

# Data used in the present study and their reduction

### 2.1 Datasets used in the present study

The vast number of discovered eclipsing binaries in nearby galaxies came as a by-product of several surveys focused on gravitational lensing, such as the EROS experiment Microlensing Survey, the Massive Compact Halo Objects (MACHO) project, the Microlensing Observations in Astrophysics (MOA), and more recently the Optical Gravitational Lensing Experiment (OGLE). The purpose of these projects, for which 1 meter class telescopes were used, was to find halos of dark matter mainly around SMC and LMC. Many newly discovered variable stars including hundreds of eclipsing binaries then renewed interest in precise distance determination of these satellite galaxies. The I-band light curves used as one of the datasets in the present study come from the OGLE II catalogue (<http://ogledb.astrouw.edu.pl/~ogle/photdb>) [31].

Purpose of several recent observations using 4-8 meter class telescopes was to obtain spectra for at least some of the objects for which the light curves are known, as both photometry and spectroscopy are needed for distance determination.

Harries et al. [15] and Hilditch et al. [16] analyzed spectra of 50 SMC eclipsing binaries of spectral types O and B, obtained with the 2dF multi-object spectrograph on the 3.9-m Anglo-Australian Telescope (AAT). Multi-object spectrograph is fed with a number of optical fibres which allow for measuring spectra of many objects at once in a certain field of view. According to [22], this was the first use of multi-object spectroscopy for objects outside the Galaxy. Radial velocities of the selected stars found out by Harries et al. [15] were intended to be used as one of the datasets in the present study, but were later discarded because of their large scatter compared to the velocities calculated from the Very Large Telescope (VLT) spectra.

North et al. [22] analyzed spectra of 33 objects from the SMC, obtained by the 8.2-m VLT FLAMES facility (also a multi-object spectrograph). Reduced and calibrated spectra of all the objects including 3 of the selected stars were provided to us by the authors. It should be noted that the reduction by North et al. was done using an old version of reduction software, which is no longer maintained. The spectra reduced by North et al. were used for preliminary disentangling and calculation of the radial velocities, prior to my



Table 2.1: Spectroscopic observations: number of the exposure, heliocentric Julian dates at mid exposure, exposure times, air mass at mid exposure, average seeing and days elapsed since the last full moon (taken from [22])

Exposure	HJD (-2450000)	$t_{exp}$ (s)	Air mass	Seeing (")	Moon age (d)
1	2959.5423	2595	1.526	0.77	21.00
2	2959.7115	2595	1.744	0.53	21.16
3	2960.5394	2595	1.526	1.27	21.96
4	2960.6778	2595	1.645	0.95	22.09
5	2961.5336	2595	1.529	0.80	22.94
6	2961.7090	2595	1.755	0.96	23.12
7	2962.5435	2595	1.519	1.00	23.97
8	2962.7269	2595	1.845	0.67	24.16
9	2963.5335	2595	1.524	1.01	25.02
10	2964.5358	707	1.518	0.98	26.13
11	2964.5560	2595	1.512	0.83	26.14
12	2964.7501	2595	1.998	0.74	26.35
13	2965.5287	2595	1.523	0.94	27.23
14	2965.7037	2595	1.779	0.92	27.43
15	2966.5454	2595	1.514	0.68	28.40
16	2966.7002	2595	1.778	1.02	28.58

Table 2.2: The reduced spectra: signal-to-noise ratio, signal-to-noise ratio of spectra reduced by North et al. [22], number of spectra used (out of 16), number of spectra used by North et al.

Object	S/N	S/N <sub>N</sub>	n <sub>sp</sub>	n <sub>sp,N</sub>
4 163552	90-171	73-132	16	9
5 038089	112-234	128-216	16	11
5 123390	98-195	91-179	16	14
6 017316	85-181	-	16	-

stay at ESO (European Southern Observatory) Vitacura office in Santiago, Chile, where I received training in reduction of raw data from the FLAMES spectrograph using an up-to-date reduction software. The improvement in the reduction process can be seen from slightly improved values of S/N ratios of the reduced spectra (Tab. 2.2). The spectra reduced and calibrated by myself were used as the main dataset complementing the OGLE photometry.

Fundamental parameters and distances of 5 OB eclipsing binaries were also determined in a recent work by Drechsel & Nesslinger ([5]).

## 2.2 Reduction of raw data from the FLAMES/GIRAFFE multi-object spectrograph

FLAMES (Fibre Large Array Multi Element Spectrograph) (Fig. 2.1) [25] is the multi-object, intermediate and high-resolution fibre facility located at the Very Large Telescope, ESO's premier site for observations in the visible and infrared light at Cerro Paranal, Chile. It is mounted at Nasmyth A platform of UT2 (Kueyen Telescope) and offers a circular field of view with 25 arcmin diameter. It consists of a Fibre Positioner (OzPoz) hosting two circular plates, each of which can host up to 560 optical fibres, which are attached to the plates with magnetic buttons. The two plates allow for limiting the dead time between observations: While one plate is observing, the other one is positioning the fibres for subsequent observations. The fibres are feeding two different echelle spectrographs covering the whole visible range: The high-resolution UVES spectrograph with eight fibres connected to each plate and a medium-high resolution GIRAFFE spectrograph. The latter is equipped with two echelles, allowing to choose between low and high resolution, and interference order sorting filters allowing to select the required spectral range (6000–10000 Å in low resolution and 2000–4000 Å in high resolution). GIRAFFE fibre feeding system is equipped with 2 MEDUSA fibre slits (one for each plate), by which up to 132 separate objects (including sky fibres which can be later used for sky subtraction) can be observed, 2 IFU (Integral Field Unit) slits for a total aperture of 3x2 arcseconds and 1 ARGUS slit, a large integral unit with a total aperture of 12x7 arcseconds. A coordinating observing software allows for simultaneous UVES and GIRAFFE observations. In the present study, only spectra from GIRAFFE using the MEDUSA fibre slits were used.

The data that were acquired by North et al. [22], originating from the observing program 0.72.A-0474A, are available for download after registration from the ESO archive ([http://archive.eso.org/eso/eso\\_archive\\_main.html](http://archive.eso.org/eso/eso_archive_main.html)). The spectroscopy was acquired on eight consecutive nights, from 2003 November 16 to 23. The spectrograph was used in the low resolution (LR2) Medusa mode: resolving power  $R = 6400$ , bandwidth  $\Delta\lambda = 6030$  Å centered on 4272 Å. One field in SMC and one in LMC were observed in turn (only objects from the SMC field are used in the present study) at a rate of 4 exposures per night with integration time of 2595 s (only the tenth exposure had integration time only 707 s due to a technical problem). So, overall 16 spectra per target were acquired for 104 targets in SMC and 44 targets in LMC (analysis of 33 SMC objects only has been published so far). Additionally, 21 sky spectra for each exposure in SMC were obtained. Further information about the spectroscopic observations is listed in Tab. 2.1.

The whole reduction process of the FLAMES data was done by myself during a three-months stay as an interim student in the ESO Vitacura office. Packages of software used for reduction of the raw data are called data reduction pipelines, and there are different ones for most VLT instruments and their specific setups. Data reduction pipelines have three main purposes: Monitoring the instrument performance, producing master calibration products from the raw calibration images (combined bias frames, super-flats, wavelength dispersion solutions) and creating science products by using the pipeline-generated master calibrations. The GIRAFFE data reduction pipeline [8] is available at

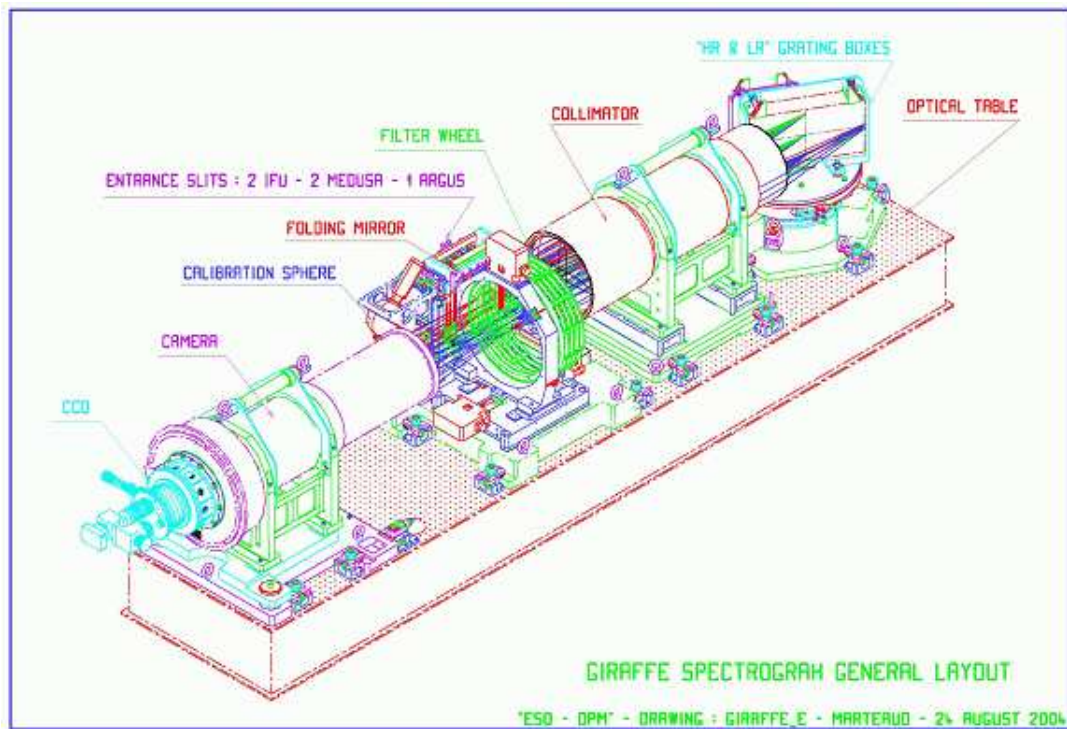


Figure 2.1: GIRAFFE Spectrograph layout

<http://www.eso.org/sci/software/pipelines/giraffe/giraf-pipe-recipes.html>. It contains the data processing modules called recipes, together with two applications which can be used for running them (Gasnano and EsoRex) and several additional libraries. Downloading the GIRAFFE Standard Calibration Data Sets is also crucial for running the pipeline recipes.

GIRAFFE data can be separated into raw frames (unprocessed outputs of the GIRAFFE instrument) and product frames (results of GIRAFFE pipeline processing). After scientific observations are made at night, raw calibration images for the specific configurations are taken during the following day. For each observing night, matching raw calibration data may be downloaded in addition to the raw images containing science observations. One would not necessarily need to do this and could use the calibration images included in the Standard Calibration Data Set (averaged calibration files), but that should serve only as a first, quick-look result.

Raw FITS (Flexible Image Transport System) files generated by the GIRAFFE instrument include the image data stored in the primary data unit and two binary table extensions: The OzPoz table containing the list of magnetic buttons placed on one of the fibre positioner plates and a FLAMES FIBRE table containing the fibre description specifying the association between fibre buttons, fibre positions in the slits and also lab-measured fibre transmission values (as the fibres usually differ from one another). While the OzPoz table is, naturally, variable from observation to observation, the FLAMES FIBRE table is static. Product images contain an extension table called FIBRE\_SETUP, which contains merged information from both extensions of the raw images.

The best option for sorting both the raw and product images is probably to use a

graphical interface application Gasgano [1]. While for running the recipes Gasgano can be used as well, I used a command-line controlled application EsoRex (<http://www.eso.org/sci/software/cpl/esorex.html>).

The steps needed to be carried out for a proper data reduction are the following: subtracting the bias and dark frames, locating fibres on the detector, applying flat-field and fibre-to-fibre transmission correction, applying dispersion solution to establish a wavelength scale and finally extracting the individual spectra. In the case of GIRAFFE, this means firstly creating master calibration products by running the recipes `gimasterbias`, `gimasterdark`, `gimasterflat` and `giwavecalibration` in that order and then using the master calibrations on the raw science frames using the recipe `giscience`. The extraction of individual spectra from the final cube product frame can be done e.g. with IRAF (Image Reduction and Analysis Facility).

Each recipe has a number of required and optional input frames, one or more output frames and a lot of adjustable parameters. For details about the recipes and their parameters, one should consult the GIRAFFE Pipeline User Manual [8].

The first step in the reduction process is to download the raw science data and matching raw calibrations. The raw calibrations include (for each night): 5 raw bias frames, 3 raw flat-field frames (Fig. 2.2) for each slit and a ThAr arc lamp spectrum (also for each slit) later used for a proper wavelength calibration (Fig. 2.2). The first recipe to run then is `gimasterbias`. It takes the set of raw bias frames and produces a master bias and optionally a map of bad detector pixels to be (also optionally) used in subsequent steps. The bad pixel map should be created if it differs from the bad pixel map present in the static calibrations. Running the `gimasterdark` recipe can usually be skipped, as subtracting the master dark frame is not strictly necessary for modern CCD detectors. The recipe to follow is `gimasterflat`. This recipe creates a master flat-field from a set of raw flat-fields, but more importantly it detects the fibres on the master flat-field and records the location and width of corresponding spectra in the calibration products called the localisation centroid frame and the localisation width frame. With the fibre positions and width, also an extracted and normalised flat-field is created. Two static calibration frames are required for `gimasterflat`: the slit geometry template and the grating physical parameters. The following `giwavecalibration` recipe takes the fibre positions obtained from `gimasterflat` and calculates a dispersion solution from the arc lamp spectrum. An optional output is the setup specific slit geometry table, which can be used subsequently instead of the static slit geometry table, should the wavelength solution be bad (Fig. 2.2). The following `gistandard` recipe is relevant only to IFU and Argus observations, primarily to monitor the instrument health. The final step is then to use the master calibration products by the recipe `giscience`, results of which are bias corrected, (optionally) dark subtracted, wavelength calibrated spectra corrected for fibre-to-fibre transmission and pixel-to-pixel variations. A fine tuning of the wavelength scale is done if simultaneous calibration lamps were used during the observations and the barycentric, heliocentric and geocentric corrections are computed for the individual spectra if the object positions are available.

In our specific case, I decided to use a new bad pixel map created by the recipe `gimasterbias` instead of a static one. However, I did not use the master bias frame itself in the other recipes, because of a 'history effect' of biases taken before July 7th 2008, which meant that not all the biases had the same flux. In subsequent steps, I subtracted the

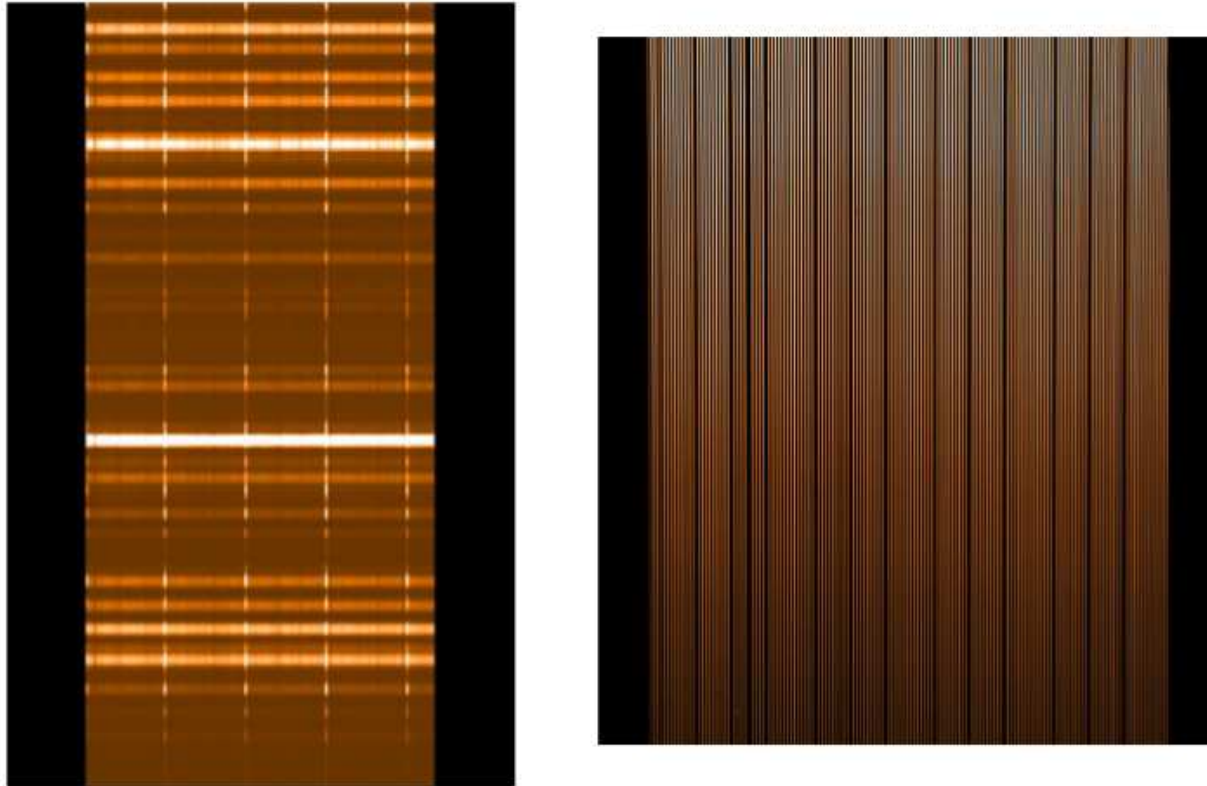


Figure 2.2: On the right: A raw flat-field frame. The vertical lines represent individual fibres with dispersion along the vertical direction. Thirteen subslits are visible with one broken fibre in the third subslit from the left (taken on November 16 2003). On the left: Part of a rebinned arc lamp spectrum (product of a raw lamp spectrum taken on November 16 2003). If the lines were not straight in the horizontal direction, a new slit geometry setup would have to be created by the giwavecalibration recipe.

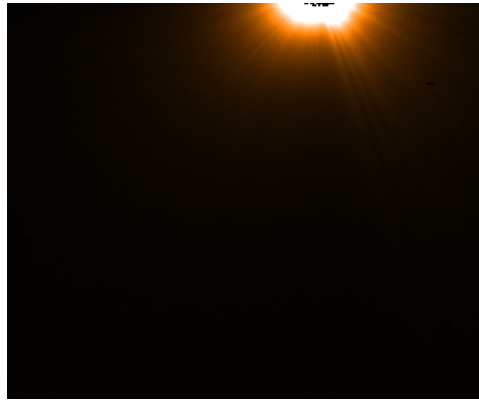


Figure 2.3: Static master dark frame: detail of a glow feature in the upper right part of the CCD detector Bruce

static master dark frame, as the observations were done by an old CCD Bruce, which had a prominent glow feature in the upper right part (Fig. 2.3) and which was later exchanged for a new CCD Carreras (for which the dark subtraction is no longer necessary). In `gimasterflat` I set the parameters to create a scattered light model (computed from the inter-spectrum regions) and then to remove the scattered light. I decided not to use a new specific slit geometry setup created by the `giwavecalibration` recipe, as the wavelength solution was good (Fig. 2.2). The final product of the `giscience` recipe, i.e. the rebinned science spectra was split into individual spectra by IRAF.

After reducing data from all observing nights I acquired 16 spectra of all 132 objects (including the sky and calibration lamp spectra). The objects to be used for further analysis were chosen on the basis of following criteria: the lowest possible S/N, well-resolved spectral lines of both components and presence of the calcium H-line.

## 2.3 Possibilities to improve the previous studies

In the analysis of the SMC eclipsing binaries by North et al. [22], disentangling of H Balmer lines was avoided because of their large width (which makes them more sensitive to systematic errors) and their possible contamination by nebular emission. The contamination allows us, however, to disentangle not only the stellar spectra but also the spectrum of circumstellar matter. North et al. also avoided the parts of spectra containing the interstellar absorption Calcium H-line. By using all the parts of spectra avoided in their study, we should be able (additionally to the goals outlined in the section 1.6) to obtain much better constrained orbital and astrophysical parameters of the binaries. North et al. also avoided the spectra taken during or near eclipses (Tab. 2.2), although they admit that Korel can in fact use the eclipsed spectra thanks to the possibility of converging the line-strength factors.

Harries et al. [15] also avoided spectra obtained during eclipses because the methods they used (they used the wavelength domain disentangling method [30]) assume that the

component spectra do not change with the orbital phase.

More importantly, the possibility of converging both photometry and spectroscopy at the same time by the Bazant code avoids the need to use intermediate results and therefore lowers error accumulation.

# Chapter 3

## Disentangling of selected spectra

### 3.1 Preparation of selected spectra for disentangling

Several crucial steps need to be done with the spectra in order to successfully begin their disentangling. These include: the sky subtraction, normalisation to continuum, correction for artifacts and smoothing. A few attempts to properly subtract the sky were made by averaging the sky spectra positioned near to the stellar object. However, the results were deemed unsatisfactory, as both the science spectra and sky spectra contain a lot of cosmic rays and instrument artifacts, resulting in the subtraction causing a distortion of some of the line profiles needed for disentangling. An option would be to manually remove the cosmics and artifacts from the sky spectra and then average them, but eventually I decided to skip the sky subtraction. This can be justified also by the fact that the selected spectra belong to bright objects, for which the sky subtraction is not so crucial. Normalisation to continuum and correction for artifacts was done using ESO-MIDAS (<http://www.eso.org/sci/software/esomidas/>).

Important conditions for successful disentangling are a signal-to-noise (S/N) ratio in the order of tens at least and a good phase coverage of the exposures. A visibility of lines of both components in the spectra is not necessary for the disentangling, however it is necessary for a precise calculation of the mass ratio and eventually the distance. The first selection of suitable spectra from the observing programme was based on the highest possible S/N ratio. After this preliminary selection, two of the stars had to be discarded, one of them because of a poor phase coverage (due to the orbital period being very close to two days) and another one because the lines of the secondary component were not sufficiently visible.

### 3.2 The disentangling procedure

Four systems were finally selected for a detailed analysis, with three of them being previously analysed by North. et al. and/or Harries and Hilditch et al. Resulting values of parameters of the object not previously analyzed are of the same precision as parameters of the other three objects (for which reliable initial guesses are available). This shows that the method may be applicable to most of the 104 SMC objects that were observed. The



analysis of all these objects is, however, far beyond the scope of this work. Analysis of additional objects will be published in a paper which is in preparation.

The analyzed stars are hot, luminous, early-type stars of spectral types O or B with an effective temperature  $\approx 30000$  K and luminosity  $\approx 10^4$  solar luminosities. With the exception of SMC 5-123390, which is slightly eccentric, all the objects have a circular orbit. The strongest lines in their spectra are the hydrogen Balmer lines and neutral helium lines. Only specific regions centered around these lines were used for the disentangling of orbital parameters. The spectral regions disentangled in this work are: 4 regions around He I lines and 3 regions around H Balmer lines with H $\gamma$  and H $\delta$  usually contaminated by the circumstellar emission and H $\epsilon$  containing also the interstellar absorption Ca H-line in its wing.

The four strong neutral helium lines were used for calculation (in a single run) of the orbital parameters. These lines are usually clearly separated during the orbital motion, because their width is smaller than that of the Balmer lines and they are not contaminated by circumstellar emission. After inserting initial guesses of the basic parameters from previous studies (where available), zero weight was given to the dataset containing spectra in order to get possibly improved values of photometry-sensitive parameters such as the period  $P$ , epoch of primary minimum  $T_0$ , radii in units of the semimajor axis  $R_{1,2}$ , inclination  $i$  and a magnitude of the primary component  $m_1$ . After that, lower weight was given to the photometry dataset and mass ratio  $q$  and velocity semiamplitude of the primary  $K_1$  (more sensitive to the spectra) were allowed to converge. Following this, the same weight was given to the two datasets and the parameters were converged again. The time difference between photometric and spectroscopic observations is useful for a more precise determination of orbital period. With the parameters fixed, the line-strength factors were calculated. For disentangling the Balmer lines H $\gamma$  and H $\delta$ , results of parameters obtained from the helium lines as well as the line-strength factors for the stellar components were used. For successful disentangling of the circumstellar component, temporary templates for the emission lines were usually needed. With the template for the third component included in the calculation, line-strength factors of all three components were converged again, and their subsequent use resulted in a good solution even after the template was removed. The line strengths of the emission lines were found to be variable, but not correlated with the orbital motion. A similar procedure as for the emission was done for the interstellar absorption line. The line strengths of the absorption are essentially different from those of the emission and were found to be more stable during the orbit.

Results of the disentangling procedure with simultaneous fitting of photometry and spectroscopy include the Keplerian orbital elements and astrophysical parameters including linear masses, radii and surface gravities. Basic parameters are listed in Tab. 3.1. The resulting values of orbital and astrophysical parameters are listed in Tables 3.2, 3.3 and 3.4. The light curves and RV curves are determined directly from the spectra and photometric data but they can also be calculated using the resulting parameters. The resulting LC and RV curves are plotted in Figures 3.2 and 3.3, with O-C in the lower parts of the figures. Some of them show a significant reduction of the O-C scatter in comparison with previous studies, as can be also seen in Tab. 3.5 and Tab. 3.6. The disentangled hydrogen Balmer lines are shown in Figures 3.4, 3.5 and 3.6.

For determination of systemic velocities, rotational velocities of the components and

most importantly the effective temperatures, we used synthetic spectra downloaded from Tlusty OSTAR2002 [20] and BSTAR2006 [21] grid of optical spectra derived for metallicity  $Z = 0.2$  and  $v_{turb} = 2\text{kms}^{-1}$  (<http://nova.astro.umd.edu/Tlusty2002/tlusty-frames-models.html>). The rectified and rebinned synthetic spectra were used as templates for the stellar components in a run of Bazant with the whole spectra included (in a lower resolution than the narrower spectral regions used for disentangling of orbital parameters). When using the synthetic spectrum as a template, the line-strength factors of the corresponding component have to be allowed to converge because the synthetic spectra are normalized to a continuum of a single star. From the resulting line-strength factors, we get an estimate on the ratio of the components' luminosities, which is otherwise obtainable only from photometry. From the relative shift of spectral lines of the observed and synthetic spectrum, Bazant calculates the systemic velocity and from the rotational line-broadening the rotational velocities of the components. A grid of synthetic spectra corresponding to different surface gravities and effective temperatures were fitted into the observed spectra and the resulting values of  $T_{eff}$  were interpolated from the best fitting ones. Fig. 3.1 shows an example of a synthetic spectrum, how it differs with changing metallicity and temperature and an example of a whole disentangled spectrum of SC5-38089.

### 3.3 Results

#### 3.3.1 SMC SC4-163552

Object previously analyzed by North et al. [22] and Harries et al. [15]. The spectra show a very narrow and unusually strong circumstellar emission in the Balmer lines, hinting at a high amount of ionized hydrogen in the surroundings of the binary. The strong emission was causing difficulties with separating the spectra of circumstellar and interstellar component from the spectra of the stellar components, as often part of the wide absorption contaminated the disentangled circumstellar lines. Unlike the remaining objects, the emission is significant also in the H $\epsilon$  line, which resulted in the need of two sets of temporary templates, one for the emission and one for the absorption. The spectra were then separated into 4 components. Photometry was solved with the presence of third light which is 0.236 mag fainter than the primary and 0.194 mag fainter than the secondary component. The resulting light curve and RV curves show a relatively low (O-C) scatter, with the RV scatter being significantly lower than in the previous studies (see Tab. 3.6).

#### 3.3.2 SMC SC5-38089

This object has also been analyzed in [22] and [15], providing us with reliable initial guesses for the stellar and orbital parameters. The spectra have the highest S/N ratio of the studied objects and possibly of all the objects obtained in the observing programme. Balmer lines H $\gamma$  and H $\delta$  are contaminated by circumstellar emission. Photometric solution includes converging of the limb darkening coefficients. A significant reduction in (O-C) of the light curve was achieved over the previous studies.

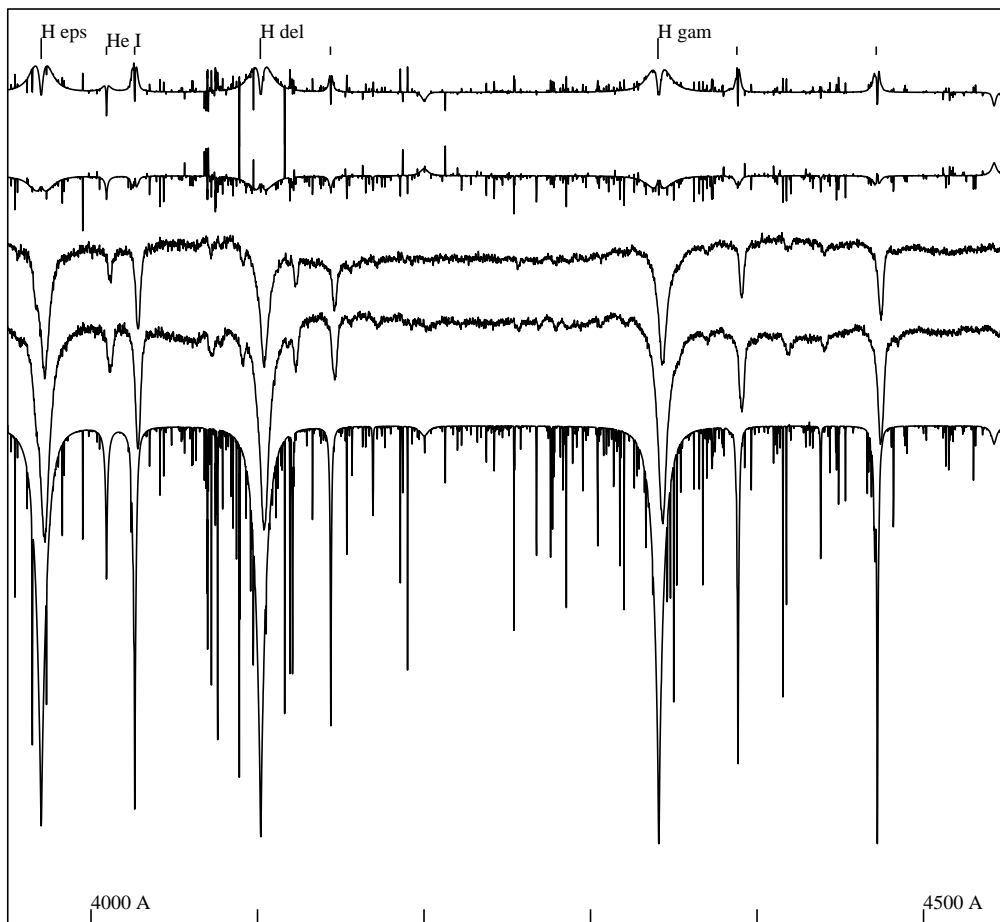


Figure 3.1: Example of a synthetic spectrum: The lowest curve shows a synthetic spectrum from the BSTAR2006 library with  $T_{eff} = 30000$  and  $\log g = 4.00$ . The upper curves show a difference between this spectrum and a synthetic spectrum with  $\log g$  being one step (0.25) lower and with  $T_{eff}$  being one step (1000 K) lower respectively. The remaining two curves are disentangled component spectra of the object SC5-38089.

### 3.3.3 SMC SC5-123390

The faintest object in our selection, previously studied in [22], also shows the shallowest eclipses. The orbit is slightly eccentric, therefore the epoch of periastron does not coincide with the epoch of primary minimum. The absence of circumstellar emission made the disentangling of Balmer lines  $H\gamma$  and  $H\delta$  easier, as the disentangling was needed for two components only and there was no need for temporary templates. The light curve and RV curve scatter are again very low with the RV scatter being significantly lower than in [22].

### 3.3.4 SMC SC6-17316

The only object previously not analysed. The shape of the light curve suggests a possibility of significant tidal distortions of the components. The radius of the primary component scaled to the semimajor axis is equal to 0.4712 and its absolute radius is almost twice as high as the radius of the secondary. This suggests that the primary has already filled its Roche lobe and a mass transfer onto the secondary is taking place. Therefore it is somewhat surprising that the light curve solution is good even when only the basic parameters (radii, inclination and the luminosity ratio) were converged. The Balmer lines  $H\gamma$  and  $H\delta$  are contaminated by a weak interstellar emission. The analysis of the object was not included in [22] for unknown reasons. However, even without the initial guesses, a reliable solution was found with the same precision as for the other objects.

Table 3.1: Basic parameters of the observed eclipsing binaries: OGLE identifying code, coordinates (J2000), orbital period, epoch of periastron and I-band magnitude

Object	$\alpha$ (h m s)	$\delta$ ( $^{\circ}$ ' ")	$P_{\text{orb}}$ (d)	$T_0$ (HJD-2450000)	$I$ (mag)
4 163552	00:47:53.24	-73 : 15 : 56.5	1.5458148	620.73053	15.7747
5 038089	00:49:01.85	-73 : 06 : 06.9	2.3894197	466.16139	15.2710
5 123390	00:49:22.66	-73 : 03 : 42.8	2.1728999	463.97478	16.2090
6 017316	00:51:40.32	-73 : 13 : 20.3	2.3238747	464.72378	15.3698

Table 3.2: Orbital parameters: eccentricity, argument of periastron, inclination, semimajor axis, mass ratio and systemic velocity

Object	$e$	$\omega_0$ ( $^\circ$ )	$i$ ( $^\circ$ )	$a$ ( $R_\odot$ )	$q = M_S/M_P$	$V_\gamma$ ( $\text{kms}^{-1}$ )
4 163552	0	90	86.70	14.70	0.9254	154.19
5 038089	0	90	76.91	18.09	0.8716	160.02
5 123390	0.032	63.01	74.07	18.87	0.8024	141.07
6 017316	0	90	64.94	17.70	0.8264	181.05

Table 3.3: Astrophysical parameters for the primary component: radius, mass, effective temperature, surface gravity and rotational velocity

Object	$R_P$ ( $R_\odot$ )	$M_P$ ( $M_\odot$ )	$T_{\text{eff}}^P$ (K)	$\log g_P$	$v_{\text{rot}}^P$ ( $\text{kms}^{-1}$ )
4 163552	5.27	9.29	24844	3.9615	218
5 038089	5.03	13.63	31181	4.1691	162
5 123390	4.24	10.59	30109	4.2078	129
6 017316	8.34	7.60	29000	3.4766	203

Table 3.4: Astrophysical parameters for the secondary component

Object	$R_S$ ( $R_\odot$ )	$M_S$ ( $M_\odot$ )	$T_{\text{eff}}^S$ (K)	$\log g_S$	$v_{\text{rot}}^S$ ( $\text{kms}^{-1}$ )
4 163552	5.16	8.60	24455	3.9475	193
5 038089	6.15	11.88	30130	3.9346	136
5 123390	3.66	8.50	30458	4.2405	104
6 017316	4.84	6.28	30000	3.8662	265

Table 3.5: Light curves: depth of primary minimum, ratio of the primary minimum to the rms, rms scatter, rms scatter from [22]

Object	$\Delta I_{\text{minI}}$ (mag)	$\Delta I_{\text{minI}}/\sigma_I$	$\sigma_I$	$\sigma_{I,\text{North et al.}}$
4 163552	0.47	52.2	0.009	0.009
5 038089	0.30	42.9	0.007	0.014
5 123390	0.75	75.0	0.010	0.010
6 017316	0.30	33.3	0.009	-

Table 3.6: Radial velocity curves: velocity semiamplitudes of the primary and secondary component, rms scatters and rms scatters from [22]

Object	$K_P$ ( $\text{kms}^{-1}$ )	$K_S$ ( $\text{kms}^{-1}$ )	$\sigma_P$	$\sigma_S$	$\sigma_{P,\text{North et al.}}$	$\sigma_{S,\text{North et al.}}$
4 163552	231.03	249.65	1.88	1.75	10.5	8.8
5 038089	212.64	243.96	2.11	2.52	3.1	2.9
5 123390	188.17	234.50	2.19	3.80	8.4	14.1
6 017316	158.34	191.61	2.89	2.09	-	-

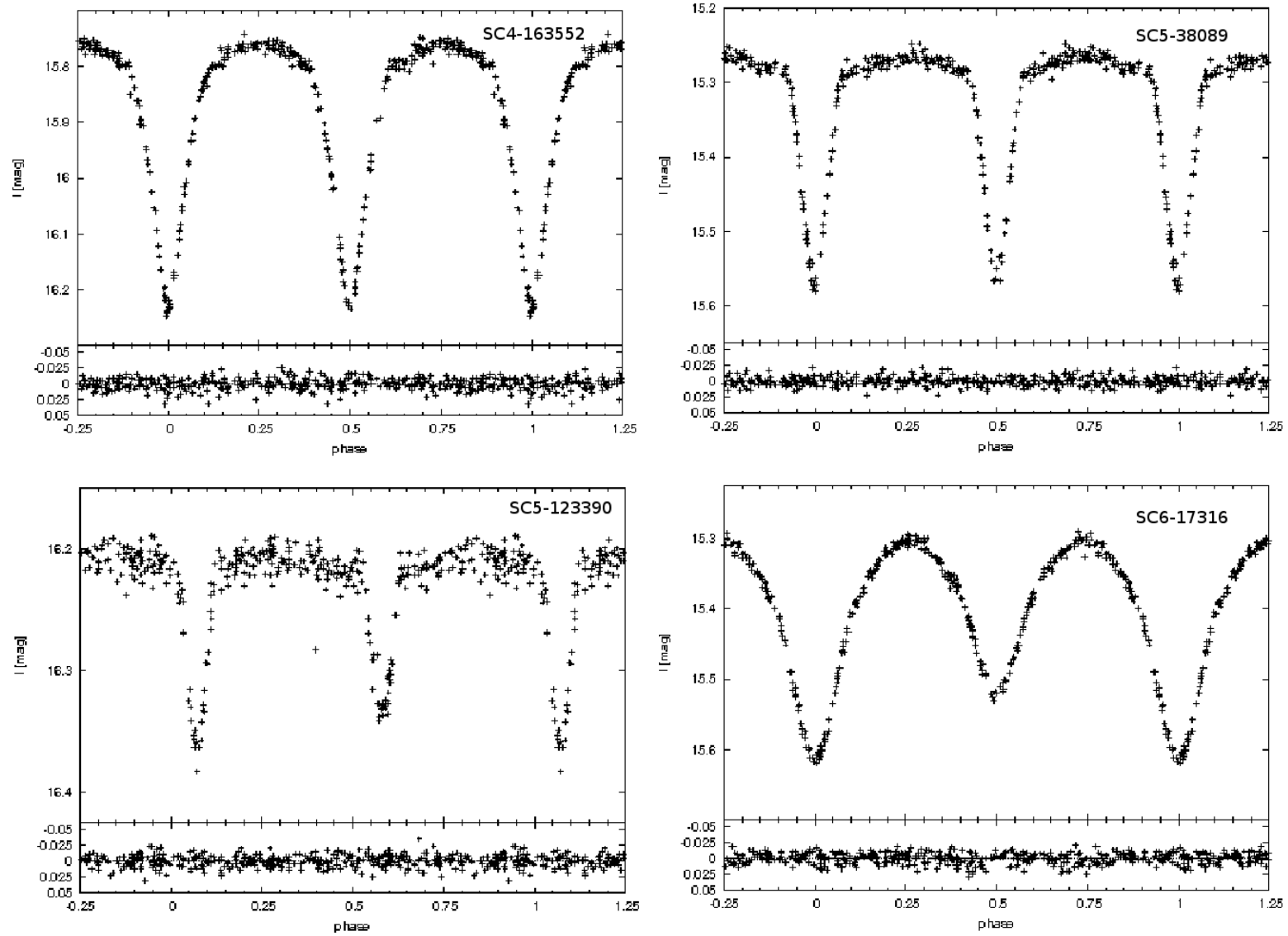


Figure 3.2: Light curves with (O-C) scatter in the lower parts of the plots.

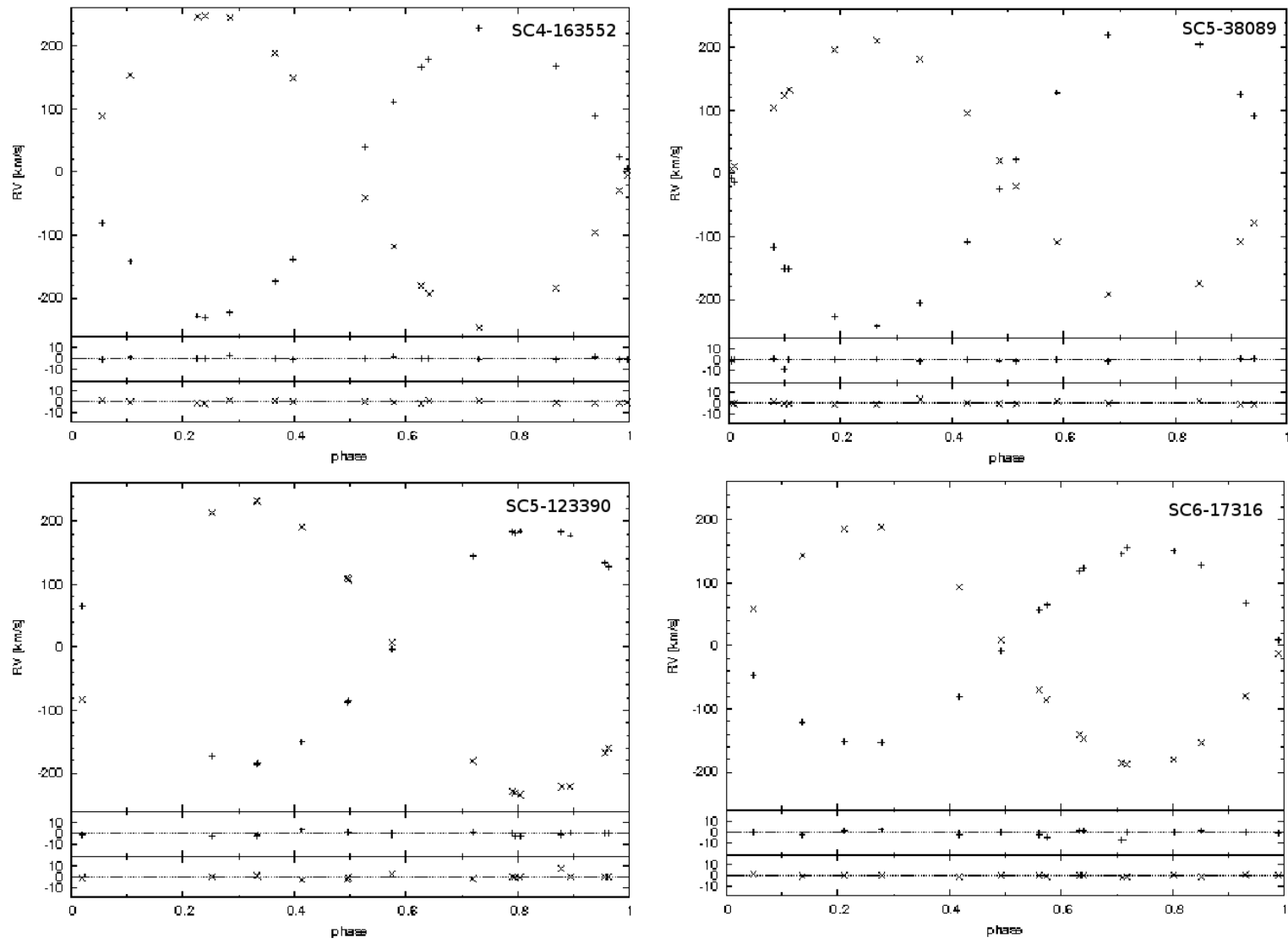


Figure 3.3: Radial velocity curves with (O-C) scatter for the primary and secondary respectively in the lower parts of the plots.

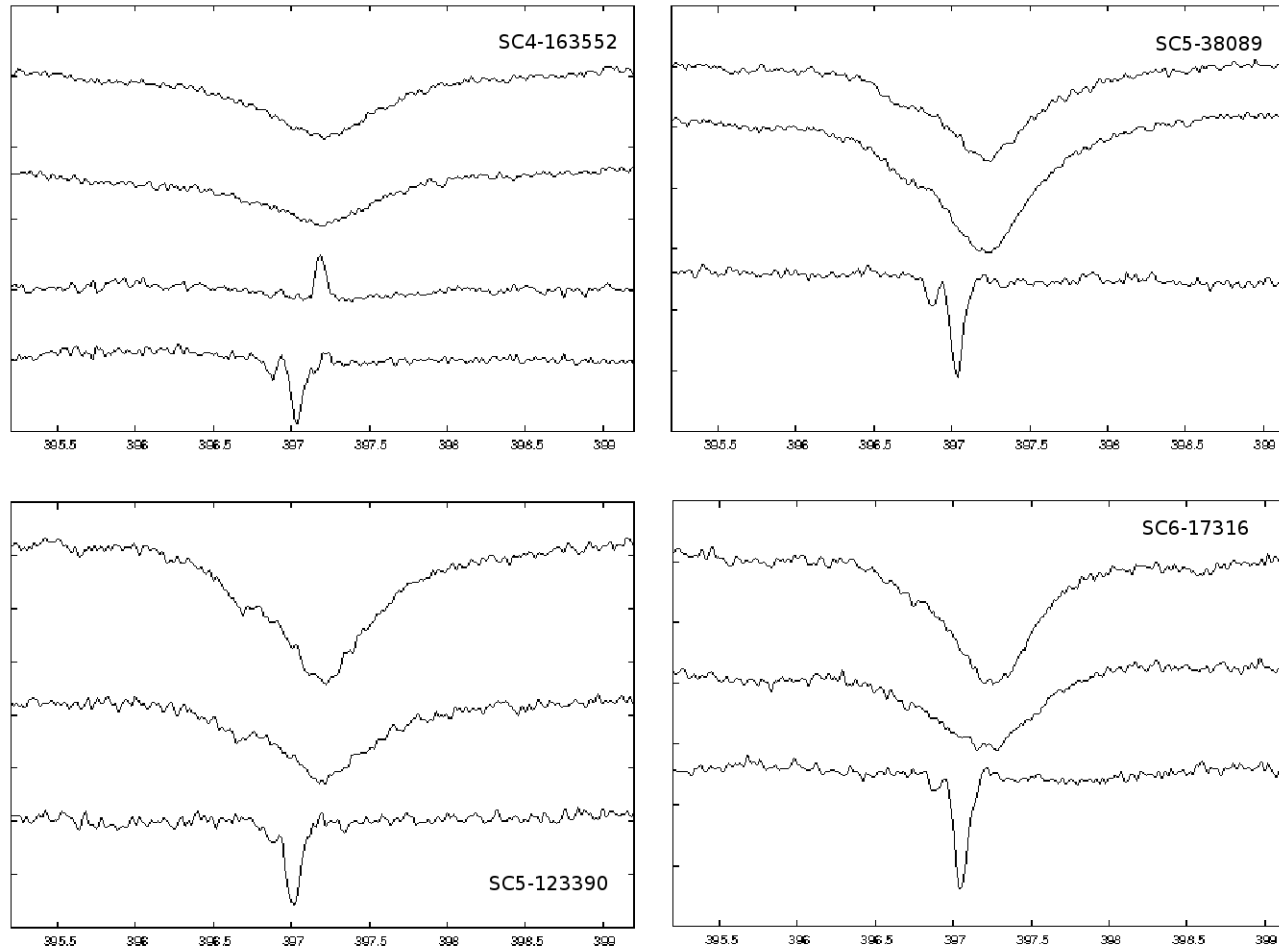


Figure 3.4:  $H\epsilon$  with the disentangled interstellar absorption line. In the case of SC4-163552, also the nebular emission had to be disentangled. One tick mark on the y-axis represents one tenth of the continuum level.



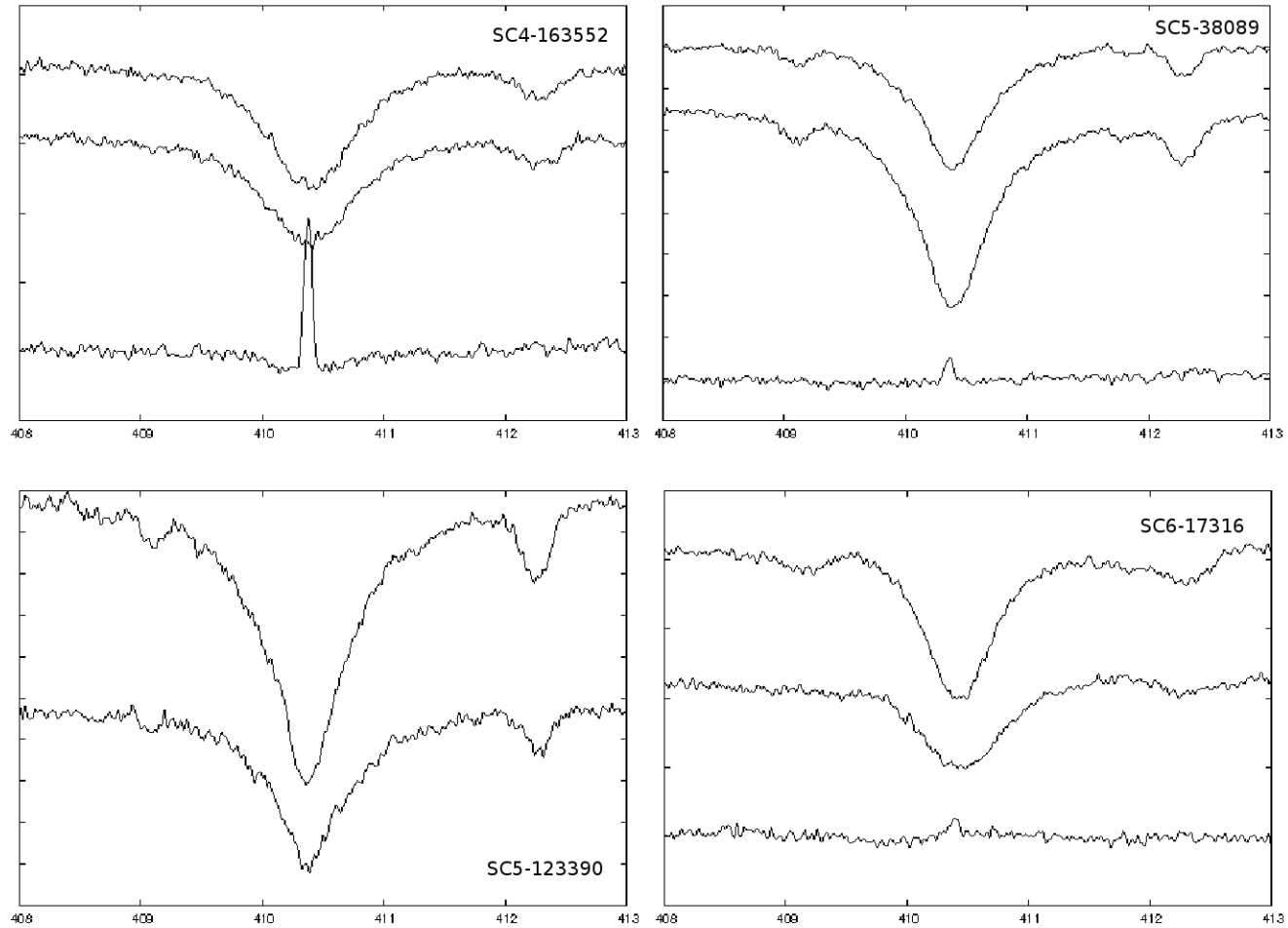


Figure 3.5: H $\delta$  with the disentangled nebular emission line (SC5-123390 is devoid of nebular emission). One tic mark on the y-axis represents one tenth of the continuum level.

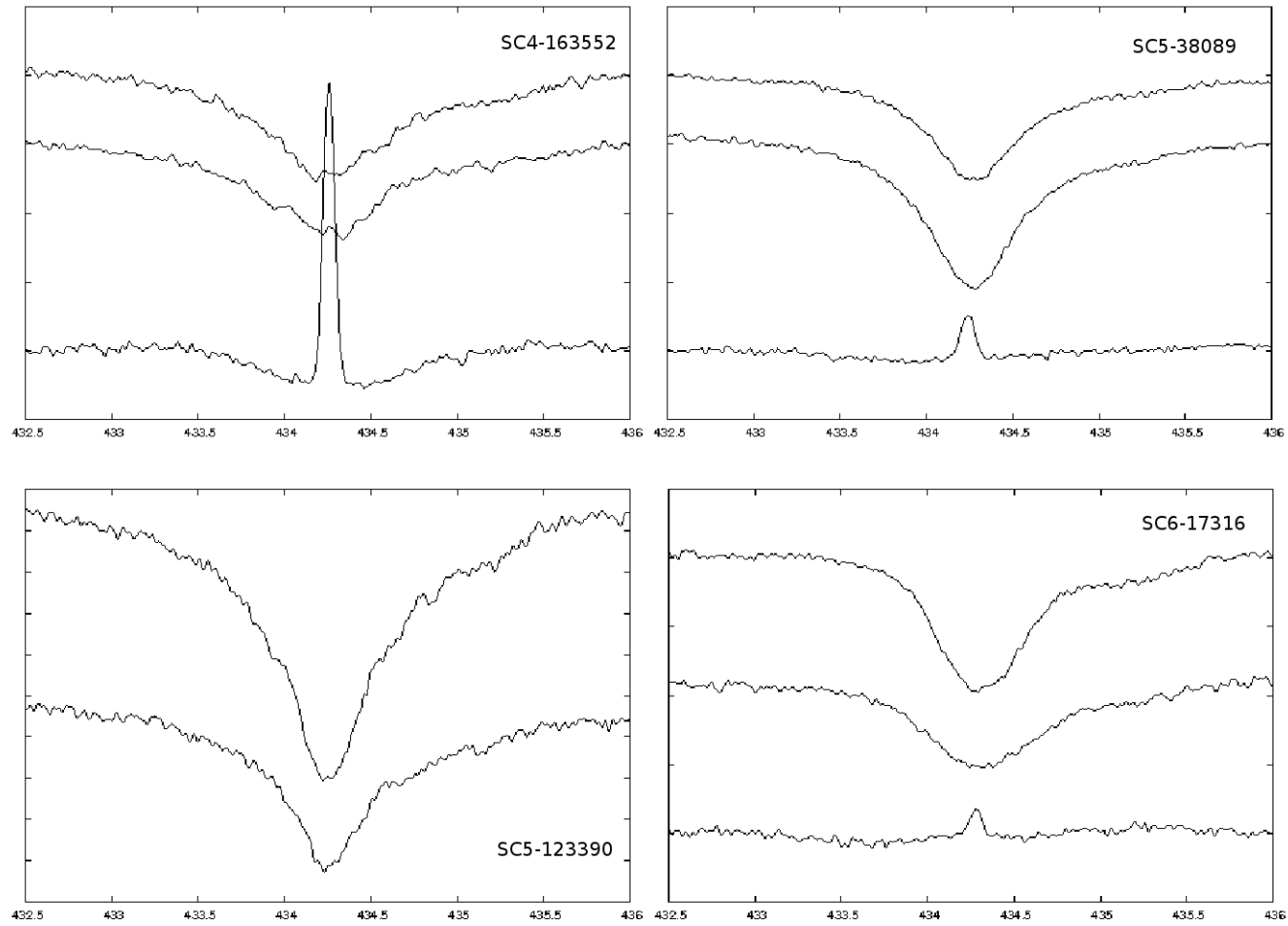


Figure 3.6: H $\gamma$  with the disentangled nebular emission line (SC5-123390 is devoid of nebular emission). One tic mark on the y-axis represents one tenth of the continuum level.

# Chapter 4

## Distance determination

### 4.1 The method used for the calculation of distance

The distances have been determined in the way described in North et al. [22]. The following equation was used for the distance modulus calculation:

$$5 \log d - 5 = I^q - M_V^q + (V - I)_0^q - 0.600A_V^q, \quad (4.1)$$

where  $I$  is the I-band magnitude,  $M_V$  is the visual absolute magnitude,  $V - I_0$  is the intrinsic colour index, and  $A_V$  is the visual extinction present in the relation  $R_V \equiv A_V / E_{B-V}$ , where  $R_V$  is the extinction parameter assumed to have a standard value of 3.1 and  $E_{B-V} = (B - V) - (B - V)_0$  is the colour excess. The superscript  $q$  denotes values at quadrature. As we were calculating with the I-band photometry only, the colour excess could not be determined, so the values of  $A_V$  calculated by North et al. [22] were adopted. The correctness of the factor 0.600, calculated by North et al. from the ratio of the absorptions in the infrared and optical bands will be questioned in the paper in preparation. The absolute visual magnitudes  $M_V^{P,S}$  of the components were determined from

$$M_V^{P,S} = M_{bol}^{P,S} - BC_V^{P,S}, \quad (4.2)$$

where  $BC_V^{P,S}$  are the bolometric corrections interpolated by North et al. from the bolometric corrections calculated by Lanz & Hubeny [20, 21]:

$$BC_V \approx 21.72 - 5.51 \log T_{eff}. \quad (4.3)$$

The absolute bolometric magnitudes  $M_{bol}^{P,S}$  were determined from

$$M_{bol}^{P,S} = -2.5 \log \left( \frac{R^{P,S}}{R_\odot} \right)^2 \left( \frac{T_{eff}^{P,S}}{T_{eff,\odot}} \right)^4 + M_{bol,\odot}, \quad (4.4)$$

with  $M_{bol,\odot} = 4.74$  mag and  $T_{eff,\odot} = 5781$  K [2]. The intrinsic colour indices  $(V - I)_0$  were calculated by North et al. from the fluxes of synthetic spectra from the BSTAR2006 library for stars cooler than 30000 K and from the fluxes by Kurucz (<http://kurucz.harvard.edu.grids.html>) for stars hotter than 30000 K, as the OSTAR2002

Table 4.1: Distance determination: visual absolute magnitude, bolometric correction, intrinsic color index, distance modulus, and distance modulus derived by North et al. [22]

Object	$M_V^P$ (mag)	$M_V^S$ (mag)	$BC_V^P$ (mag)	$BC_V^S$	$(V - I)_0$	DM	$DM_N$
4 163552	-2.72	-2.62	-2.48	-2.47	-0.246	18.60	18.36
5 038089	-3.11	-3.37	-2.98	-3.01	-0.292	18.30	18.83
5 123390	-2.79	-2.47	-2.78	-2.83	-0.274	19.16	18.76
6 017316	-4.00	-2.89	-2.87	-2.95	-0.285	19.09	-

library does not give fluxes beyond 7500 Å. The following first-order approximation was used:

$$(V - I)_0 \approx 0.502 - 0.178 \log T_{eff}. \quad (4.5)$$

The resulting values of the distance moduli and other quantities used for the distance determination are listed in Tab. 4.1. Note that the value of the distance modulus for SC6-17316 represents its upper limit. As it was not included in the analysis by North et al., the visual extinction  $A_V$  for this object was not available and a coloured photometry would be needed for its calculation. If we use an average of the 32 values (for one of the objects, coloured photometry was not available) for the objects studied in [22] ( $A_{V,average} = 0.41$ ), the distance modulus would become 18.85.

## 4.2 Conclusions

Raw data from the FLAMES/GIRAFFE multi-object spectrograph containing 16 spectra of 104 eclipsing binaries in the SMC, have been reduced. With the inclusion of OGLE I-band photometry, absolute orbital and astrophysical parameters were derived for 4 of these objects, one of which has not been analyzed before. There are several reasons to believe that our results represent an improvement in the accuracy of the resulting values of parameters over the study of North et al. [22], where analysis of 33 of the 104 objects has been published. Our spectra have a higher S/N ratio due to the use of an updated reduction software and our method allowed the use of spectra obtained during eclipses, while North et al. in some cases discarded up to almost half of the spectra for being taken during or near eclipses (Tab.2.2). To determine the parameters, we were converging both photometry and spectroscopy at the same time by the new code Bazant, which also represents a significant improvement over any of the previous studies. Apart from determining the stellar and orbital parameters from the 4 neutral helium lines, hydrogen Balmer lines contaminated by nebular emission (apart from the object SC5-123390) and an interstellar H-line of ionized calcium were disentangled (Figures 3.4, 3.5 and 3.6). However, our distance moduli may suffer from an error accumulation, as values of several parameters such as the visual extinction and the colour indices were adopted from [22] although they could have been determined more precisely if we used photometry from different colour bands.

Several aspects of the method will be looked into in more detail in a paper which is in preparation. Already mentioned is the inclusion of coloured photometry and revising some steps in the distance determination done by North et al. [22]. Disentangled interstellar absorption line in the 4 objects will also be studied in more detail. Apart from providing us with the upper limit on the distance of the interstellar medium (the distances of the binaries), the disentangled lines will also provide us with the estimate of the column density of the interstellar matter. Their equivalent widths and line-profiles will be compared with the extinction, the distance and possibly the 21cm HI profile. The uncertainties of the resulting parameters will also be looked into in more detail, as their determination can be a rather complex task.

# Bibliography

- [1] Amico P., Kornweibel N., Zamparelli M.: *Gasgano User's Manual*, Doc. No. VLT-PRO-ESO-19000-1932, (2001).
- [2] Bessell M. S., Castelli F., Plez, B.: *Model atmospheres broad-band colors, bolometric corrections and temperature calibrations for O - M stars*, *Astronomy & Astrophysics*, **333** (2001) 231–250.
- [3] Bonanos A.Z.: *Eclipsing Binaries: Tools for Calibrating the Extragalactic Distance Scale*, IAU Symposium No. 240, (2006).
- [4] Brüns C. et al.: *The Parkes H I Survey of the Magellanic System*, *Astronomy & Astrophysics*, **432**, (2005) 45–67.
- [5] Drechsel H., Nesslinger S.: *Accurate Fundamental Parameters of Five OB-type Systems in the SMC*, *ASP Conference Series* **435**, (2010) 381.
- [6] Feast M.: *The Current Status of Primary Distance Indicators*, *ASP Conference Series* **329**, (2005) 241.
- [7] Graczyk D.: *Light-curve solutions for bright detached eclipsing binaries in the Small Magellanic Cloud: absolute dimensions and distance indicators*, *Mon. Not. R. Astron. Soc.* **342**, (2003) 1334–1348.
- [8] GIRAFFE Pipeline Team: *GIRAFFE Pipeline User Manual*, VLT-MAN-ESO-19500-3883 **4**, (2010).
- [9] Hadrava P.: *Orbital elements of multiple spectroscopic stars*, *A&A Supplement* **114**, (1995) 393.
- [10] Hadrava P.: *Relative line photometry of eclipsing binaries*, *A&A Supplement* **122**, (1997) 581–584.
- [11] Hadrava P.: *Disentangling of spectra of multiple stars*, *ASP Conference Series* **318**, (2004) 86–94.
- [12] Hadrava P.: *Disentangling of spectra - theory and practice*, eprint arXiv:0909.0172, (2009).
- [13] Hadrava P.: *FOTEL 4 - User's guide*, *Publications of the Astronomical Institute of the Academy of Sciences of the Czech Republic (ISSN 1211-9105)*, **92**, (2004) 1–14.

- [14] Hadrava P. et al.: *Notes on disentangling of spectra - II. Intrinsic line-profile variability due to Cepheid pulsations*, *Astronomy & Astrophysics* **507**, (2009) 397–404.
- [15] Harries T.J., Hilditch R.W., Howarth I.D.: *Ten eclipsing binaries in the Small Magellanic Cloud: fundamental parameters and Cloud distance*, *Mon. Not. R. Astron. Soc.* **339**, (2003) 157–172.
- [16] Hilditch R.W., Howarth I.D., Harries T.J.: *Forty eclipsing binaries in the Small Magellanic Cloud: fundamental parameters and Cloud distance*, *Mon. Not. R. Astron. Soc.* **357**, (2005) 304–324.
- [17] Hill G.: *The Measurement of Radial Velocities Using Cross-Correlation Techniques as Applied to Binary Stars*, *New frontiers in binary star research : a colloquium sponsored by the U.S. National Science Foundation and the Korean Science and Engineering Foundation, Seoul and Taejon, Korea, November 5-13, 1990*. Edited by Kam-Ching Leung and Il-Seong Nha. San Francisco, Calif. Astronomical Society of the Pacific, (1993) 127.
- [18] Kallrath J., Linnell A.P.: *A new method to optimize parameters in solutions of eclipsing binary light curves*, *Astrophysical Journal*, Part 1 (ISSN 0004-637X) **313**, (1987) 346–357.
- [19] Kruszewski A., Semeniuk, I.: *Nearby Hipparcos Eclipsing Binaries for Color - Surface Brightness Calibration*, *Acta Astronomica* **49**, (1999) 561–575.
- [20] Lanz T., Hubeny, I.: *A Grid of Non-LTE Line-blanketed Model Atmospheres of O-Type Stars*, *The Astrophysical Journal Supplement Series* **146**, (2003) 417–441.
- [21] Lanz T., Hubeny, I.: *A Grid of NLTE Line-blanketed Model Atmospheres of Early B-Type Stars*, *The Astrophysical Journal Supplement Series* **169**, (2007) 83–104.
- [22] North P. et al.: *VLT multi-object spectroscopy of 33 eclipsing binaries in the Small Magellanic Cloud*, *Astronomy & Astrophysics* **520**, (2010) A74.
- [23] Paczynski B.: *Detached eclipsing binaries as primary distance and age indicators*, *Conference Paper, Space Telescope Science Institute Series, The Extragalactic Distance Scale*, edited by M. Livio (Cambridge University Press) (1997) 273–280.
- [24] Paczynski B.: *LETTER to the EDITORS: The Distance to Pleiades*, *Acta Astronomica*, **53**, (2003) 209–211.
- [25] Pasquini L. et al.: *Installation and commissioning of FLAMES, the VLT Multifibre Facility*, *The Messenger*, **110**, (2002) 1–9.
- [26] Rucinski S.M.: *Radial Velocity Studies of Close Binary Stars. VII. Methods and Uncertainties*, *The Astronomical Journal*, **124**, (2002) 1746–1756.
- [27] Růžička, Adam, Theis, Christian, Palouš, Jan: *otation of the Milky Way and the Formation of the Magellanic Stream*, *The Astrophysical Journal*, **725**, (2010) 369–387.

- [28] Růžička, A.; Palouš, J.; Theis, C.: *Is the dark matter halo of the Milky Way flattened?*, *Astronomy & Astrophysics*, **461**, (2007) 155–169.
- [29] Stanimirovic S., Staveley-Smith, L., Jones, P.: *A New Look at the Kinematics of Neutral Hydrogen in the Small Magellanic Cloud*, *The Astrophysical Journal*, **604**, (2004) 176–186.
- [30] Simon K.P., Sturm E.: *Disentangling of composite spectra*, *Astronomy & Astrophysics*, **281**, (1994) 286–291.
- [31] Udalski A. et al.: *The Optical Gravitational Lensing Experiment. Eclipsing Binary Stars in the Small Magellanic Cloud*, *Acta Astronomica*, **48**, (1998) 563–651.
- [32] Wilson R.E.: *Eclipsing Binary solutions in physical units and direct distance estimation*, *the Astrophysical Journal* **672**, (2008) 575–589.
- [33] Zwahlen N. et al.: *A purely geometric distance to the binary star Atlas, a member of the Pleiades*, *Astronomy & Astrophysics*, **425**, (2004) L45–L48.



